

ISSN:2538-516X

Journal of
**Civil
Engineering
Researchers**

Volume: 4; Number: 3; September 2022

Chief Editorial:
Morteza Jamshidi

Managing Editor:
Kamyar Bagherineghad



J-Researchers



Volume 4, Number 3, September 2022

Contents

- | | | |
|----|---|-------|
| 1. | A Review on Buckling Restrained Braces | 1-10 |
| | Mohammad Hassan Hatampour | |
| 2. | fragility curves for steel moment frame with welded flange plate connection | 11-20 |
| | Ali Mirzaee, Mir Hamid Hosseini, Mohammad Reza mansoori | |
| 3. | Numerical evaluation of fracture behavior of split concrete beams reinforced with steel sheet | 20-30 |
| | Lobat Hosseinzadeh | |
| 4. | Experimental study of compressive strength, permeability and impact testing in geopolymer concrete based on Blast furnace slag | 31-39 |
| | Mohammadhossein Mansourghanaei, Morteza Biklaryan | |
| 5. | Seismic reliability analysis for strengthening of reinforced-concrete hospital building with base isolation Frames | 40-51 |
| | Mostafa Radmehr, Abbas Akbarpour, Muhammed Maleknia | |
| 6. | Investigation of explosive loading and its type of operation | 52-57 |
| | Samet Sadeghian | |



A Review on Buckling Restrained Braces

Mohammad Hassan Hatampour  a,*

^aMaster's student in structural engineering of Zand University, Shiraz, Iran

Journals-Researchers use only: Received date: 2022.07.01; revised date: 2022.08.09; ; accepted date: 2022.09.25

Abstract

One of the problems of common bracing system is their buckling against compressive loads, which reduces the amount of energy loss of the structure. Buckling Restrained Brace (BRB) have solved the problem of conventional braces by eliminating the overall buckling of the brace under pressure. Buckling Restrained Braced Frame (BRBF) is a new type of bracing system that has been widely used in recent years. Nowadays the use of buckling restrained braces, due to having more advantages compared to conventional steel braces, have received the attention of researchers and engineers that these advantages include: high ductility, more energy loss, no overall and local buckling, and also having a symmetrical cyclic curve. This type of bracing is considered as one of the effective systems for dealing with lateral loads caused by the earthquake. Disadvantages in the seismic behavior of conventional braces, such as ductility and low energy loss, general and local buckling, as well as having an asymmetric cyclic curve, have provided grounds for its modification or exclusion from the seismic design process. Buckling restrained braces are a type of energy loss system that, in addition to providing high lateral stiffness, increase the formability and energy loss of the structure. The use of this type of braces is allowed in the regulations of some countries. But in some other countries, including Iran, it has not been mentioned. According to the seismicity of the country and the increasing use of these structures in the world, the use and localization of this type of bracing system in Iran is inevitable, and the entry of this lateral bearing system into the design regulations, especially the earthquake regulations of Iran, is mandatory. The results of the analysis show that the energy loss capacity of the buckling restrained brace is about 5 times the energy loss capacity of the normal brace.

(DOI:<https://doi.org/10.52547/JCER.4.3.1>)

Keywords: buckling restrained brace, hysteresis behavior, energy loss, cyclic load, resistance, passive control system;

* Corresponding author. Tel.: +98 917 919 8766; e-mail: mh.hatampour@gmail.com

1. Introduction

The occurrence of an earthquake as a natural phenomenon in most regions of the world causes human casualties and structural and non-structural damages for various reasons. One of the main goals of earthquake engineering researchers is to reduce damages caused by earthquakes. Due to Iran's location on the Alpine-Himalaya earthquake belt, it is considered one of the earthquake-prone countries in the world, and based on previous experiences, the possibility of various earthquakes occurring is not far from expectation. Considering the damage caused by past earthquakes in Iran and the world on buildings, it is necessary to pay attention and use modern seismic systems in order to reduce the damage and increase the speed of the structure's return to its original state. Therefore, it is inevitable to use appropriate preparations in the lateral bearing systems of structures to reduce the damage caused by earthquakes. Today, it has been proven that the design of structures in such a way that they have fully elastic behavior to deal with severe earthquakes is not economical, as a result, methods such as passive control of structures against earthquakes are used in the design of structures. In this method, some structural members bear damages during severe earthquakes so that the damages on the main members of the structure such as columns are reduced and thus the structure is stay safe from major damages. Passive methods are generally divided into two categories: energy loss systems and base separators. bracing systems in steel frames are easier to implement and have a lower cost compared to bending frames; For this reason, they are widely used in steel buildings. However, with the occurrence of large and destructive earthquakes in the last few decades, many steel wind-braced buildings, which were designed according to the existing seismic design codes, did not show proper performance. Research has shown that many of the behavioral defects of conventional convergent braces are the result of the difference between compressive and tensile capacity and deterioration in the coaxial bracing system of these braces, which is caused by the buckling of the brace in compression mode. The weakness of coaxial braces can be corrected by using buckling restrained braces, in which the brace yields

in compression without buckling occurring. With the existence of various lateral bearing systems, Buckling-Restrained Braced Frame (BRBF) have a special place in seismic resistant systems due to their high stiffness, optimal energy absorption, and stable cyclic behavior (hysteresis). Due to the lack of buckling, they are able to dissipate a lot of energy and are used in the passive control of structures.

2. Buckling restrained braces

In general, steel braces are divided into two categories: convergent and divergent braces. The capacity of conventional convergent braces is very different in tensile and compression, especially in alternative loading such as earthquakes. Existing converging braces have an acceptable capacity in tensile, but under pressure due to the occurrence of buckling phenomenon, they do not have adequate resistance. In other words, the common convergent bracing system suffers a deterioration in resistance and stiffness in compression mode, while buckling restrained braces show good performance and their hysteresis curve is complete and stable and at the same time symmetrical, and the decrease in resistance and Their hardness is not observed.

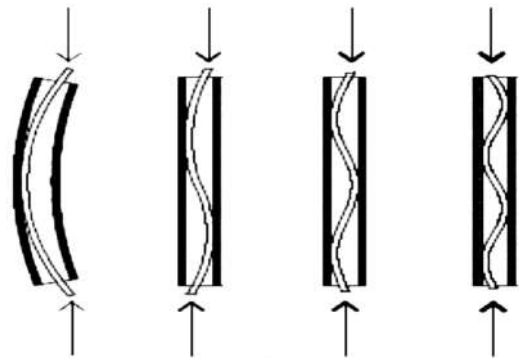


Fig.1. The idea of enclosing the column for more pressure bearing capacity. [2]

The buckling of the compression members of the common braces occurs as an undesirable behavior of the systems under the effect of secondary non-linear geometric deformations and leads to a reduction in the ductility and energy loss capacity of the structure.

Paying attention to this issue is particularly important in periodic loadings such as earthquakes due to the nature of stiffness reduction under seismic dynamic loads. Preventing the buckling of bracing members with the aim of providing compressive yielding has been investigated in India for the first time, about 30 years ago in order to prevent the buckling of columns and the increase of their loading. After that, studies on buckling restrained braces were conducted in Japan in 1980, and in 2000 in America, mentioned braces were used in practice and their application expanded rapidly.

The main principles of the operation of buckling restrained braces is to prevent the occurrence of buckling of the steel core in order to allow the phenomenon of compressive yielding to occur in it and as a result, the possibility of absorbing energy in this member of the structure. This is possible by covering the entire length of the steel core in a steel casing filled with concrete or mortar. In this system, it is necessary to provide a sliding surface or discontinuity layer between the metal core and the enclosing concrete. The main advantage of this work is to raise the buckling mode to the extent that the buckling mode of the brace occurs after the central core has occurred in pressure.

The behavior of frames with torsional buckling restrained braces, despite the appearance similarity, is very different from conventional coaxial braced frames. In the buckling restrained bracing system, the hysteresis cycles are stable and during multiple loading and unloading cycles, no drop in the resistance and stiffness of the system is observed.

3. The history of buckling restrained braces

Buckling restrained braces were first used in Japan in 1989. Today, they are widely used as seismic members in earthquake-prone areas, including in Japan, the United States of America, China, etc. In 1970, a number of researchers in Japan and India reached significant results in their research and presented the basic concepts of buckling restrained braces. Saki, Wada et al., in 1988, used steel tubes filled with mortar to restrain the buckling of the

structure, and the first buckling restrained brace was created.

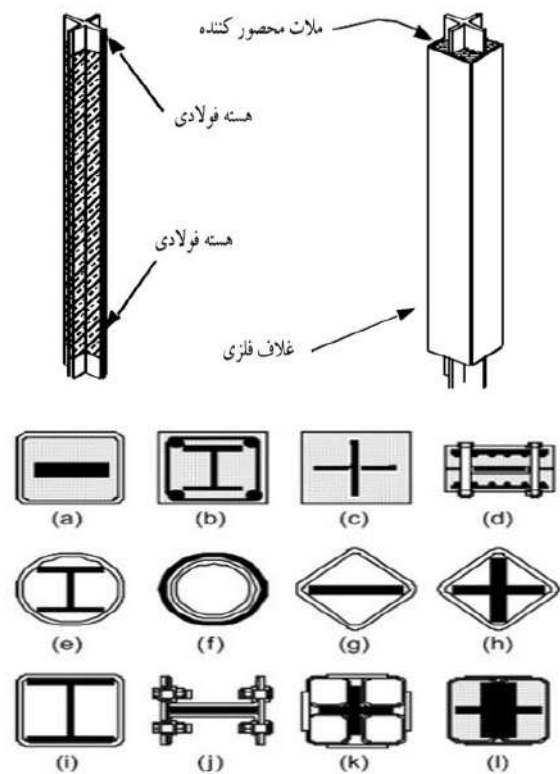


Fig.2. Constituent components and sections used in buckling restrained brace. [2],[5]

The research on buckling restrained braces in Japan and some other countries started about 30 years ago and its idea was improved during this period. The widespread use of this bracing system began after the Northridge earthquake in America in 1994 and the Kobe earthquake in Japan in 2003. By 2003, more than 250 buildings in Japan and 25 buildings in America were built with this system. This research continued after the Northridge earthquake and was expanded and advanced in terms of theory by Clark et al. in 1999, Lopez in 2001, Aiken et al. in 2002, and Sable et al. In our country, Iran, due to its location on the Alpine-Himalaya earthquake belt, research on torsional buckling restrained braces has started about 15 years

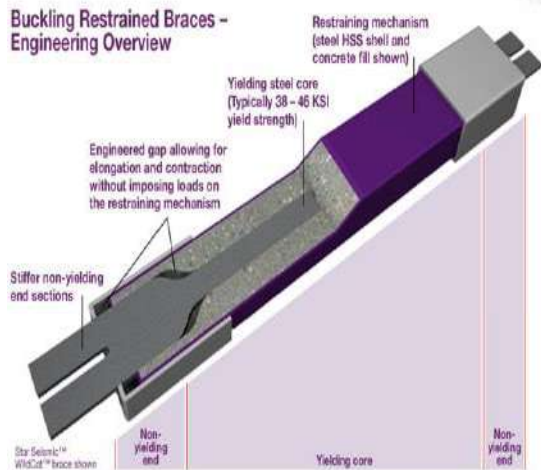


Fig. 3. Different parts of a buckling restrained brace.
[<https://sabzsaze.com/buckling-restrained-brace>]

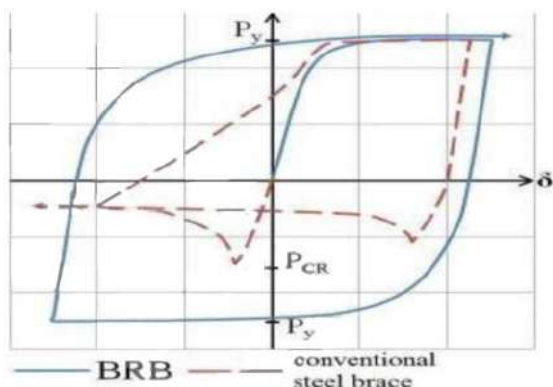


Fig. 4. Hysteresis behavior of conventional braces and buckling restrained. [6]

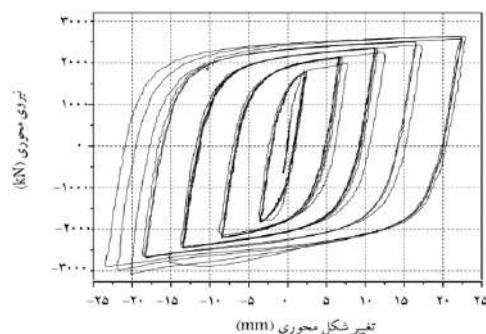


Fig.5. Cyclic curve of steel buckling restrained braces based on laboratory results. [4]

ago, and its production has been started by private sectors since 2014.

4. Evaluating the seismic behavior of steel structures with buckling restrained bracing by the scaled nonlinear dynamic analysis method

In a research conducted by Mr. Ghodrati Amiri and other colleagues in 2011, the seismic performance of steel frames with buckling restrained braces was investigated by scaled nonlinear dynamic analysis as well as nonlinear static analysis. In this research, a number of 3 and 12 story braced frames with diagonal, transverse, two-part and chevron buckling restrained braces were designed and by considering the effect of the number of earthquake records in the nonlinear dynamic analysis, the dispersion of the results was analyzed and the results show this issue that the non-linear static analysis method overestimated the response values of the buildings in some cases, and the increase in earthquake records did not have much effect on improving the dispersion of the results in the scaled dynamic method

According to the results obtained from this research, it was determined that non-linear static analysis methods have a good ability to estimate roof displacement. However, these methods are not accurate in estimating the parameters between floors (such as displacement and relative displacement), especially in buildings where the effects of higher modes are involved. For this reason, the scaled dynamic analysis method tries to use the strengths of the non-linear static method (in estimating the target location change) and the non-linear dynamic method (in estimating the response values between floors). Of course, it is necessary to note that in this research, only the frames braced with buckling restrained braces have been examined and in order to make a definite opinion about the advantages and disadvantages of this method, more and more extensive researches are needed on other types of building systems. According to the results of the analysis in this research, it can be said:

- The results of this research show that the scaled nonlinear dynamic analysis has a suitable

capability in estimating the seismic response of buildings. Therefore, this method is an efficient method when the number of records corresponding to the construction of the building is not available (such as in Iran)

- The comparison of response values of 3 and 12-story buildings in nonlinear static analysis and scaled nonlinear dynamic analysis shows that the static analysis estimates the displacement values, relative displacement and shear of the floors in these structures at the level of high performance. This article can cause uneconomic design or improvement of the structure. However, in order to make a general comment in this regard, it is necessary to examine a wider range of structures.
- In all the buildings used in this research, at the beginning of the nonlinear region (relative roof displacement 0.2%), the response values obtained from the scaled nonlinear dynamic analysis are in good agreement with the responses obtained from the equivalent static load pattern and First mode of the structure in a non-linear static method. However, with the increase in demand, the difference between the answers in the two mentioned methods increases.
- The comparison of 12-story buildings with chevron and diagonal bracing shows that the response values in the scaled nonlinear dynamic analysis method are between the response values of two equivalent and uniform static load patterns (or distribution according to the first mode of the structure). However, using two load patterns according to FEMA356 is not always reliable
- As the demand increases in the above structures, the dispersion of displacement response and relative displacement resulting from the scaled nonlinear dynamic analysis increases greatly. Also, the results show that increasing the number of earthquake records to more than 5 records in the studied structures does not have a significant effect on reducing the dispersion of the results.

5. Determination of the Parameters Influencing Behavior Factor of Buckling Restrained Braced Reinforced Concrete Frames

In the research conducted by Mr. Tasnimi and Mrs. Dehghan in 2012, the factor of behavior of reinforced concrete frames with buckling restrained braces with four, eight, twelve and sixteen story, each of which has three and five openings was designed and examined in accordance with the ninth topic of the national regulations. In this research, by using OPENSEES software, the buildings were subjected to non-linear static loading and the behavior factor of all frames was calculated for the final limit state.

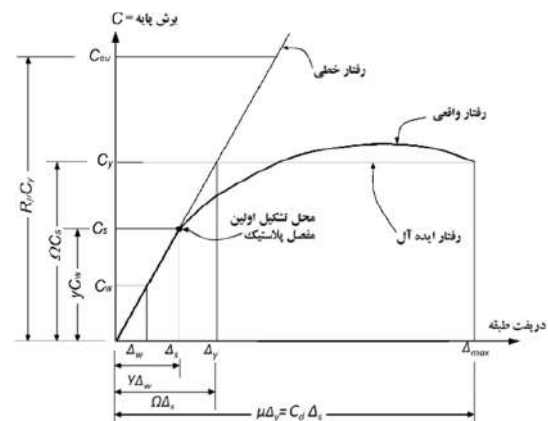


Fig.6. How to determine the behavior factor from the capacity curve. [3]

The results obtained from this research are:

- Among all the studied frames, the ductility factor of frames braced with buckling restrained brace is higher than other systems.
- Among all the studied frames, the ductility factor of frames without braces is lower than other systems.
- The average factor of ductility in frames with buckling restrained braces is around 5.
- The average factor of ductility in frames with conventional braces is around 4.
- The average factor of ductility in frames without braces is about 2.5.

- Frames with buckling restrained braces have higher ductility than other systems.
- The additional resistance factor in braced systems with normal brace and buckling restrained are close to each other.
- The lowest additional resistance factor is related to frames without braces.
- The average factor of behavior obtained for the braced system with buckling restrained brace is about 8.

6. The effect of the yield zone length on the seismic performance of buckling restrained braces

In a research conducted by Mr. Raisi Dehkordi and other colleagues in 2015, the effect of the length of the yield zone on the seismic performance of buckling restrained braces in two groups of short-story and mid-story steel buildings of 5 and 8 stories with buckling restrained bracing frames with 4 and 6 meter spans were studied. In this research, ABAQUS software was used for the nonlinear finite element model.

The results have shown that the reduction of the cross-sectional area of the buckling restrained brace has led to a reduction in the length of the yield zone and the contact surface between the core and the casing, and therefore the frictional force transmitted to the casing has also been reduced, and the length of the buckling region has also been shortened. As a result, the steel casing of the brace can be replaced with a shorter length, which will economically save costs.



Fig.7. 3D figure made in ABAQUS software for buckling restrained brace. [4]

In order to evaluate the seismic performance of structural models with buckling restrained braces, nonlinear dynamic analysis were used and loading was done according to the 2800 standard and with 3 different patterns. Using the earthquake load factor and defining the lateral load uniformly and applying loading were through acceleration mappings which was in accordance with the research conditions of different loading patterns. After performing nonlinear analysis, the obtained results have been compared with the acceptance criteria of braces.

Table 1. Acceptance criteria for buckling restrained braces. [4]

Acceptance Criteria		Performance levels
Nippon Steel	ASCE41-06	
5 Δy	0.25 Δy	Immediate Occupancy
15 Δy	11 Δy	Life Safety
20 Δy	13 Δy	Collapse Prevention

Seismic evaluation of the studied structures in this research based on the results of non-linear analysis about the reduction of material used in buckling restrained braces has led to the following results:

- The narrower the middle section of the opening of the brace is, the length of the yield zone decreases, and as a result, a smaller area of the brace reaches the yield point, and there is stress concentration in a short area, and the reliability factor is greatly reduced. Also, to any extent, the length of the brace increases, the length of the yield zone increases, but the ratio of the yield zone to the length of the brace does not change much. According to the increase in force and the proper performance of the buckling restrained braces, the force is properly distributed in them and the concentration of stress in one area and the creation of critical conditions are prevented.
- by increasing the number of floors and decreasing the cross-sectional areas, the length of the yield zone increases. It can be concluded that due to the increase in the length of the dough region, the stress is reduced and the reliability factor is

increased, which leads to the improvement of the conditions of using buckling restrained braces in taller structures.

- In the studied models, where the cross-sectional area of the braces has been reduced to 75%, the seismic demand created in the braces has increased to the extent of the change of locations corresponding to the collapse performance levels.
- In the studied models, in which the reduction of the cross-sectional area was 50%, the seismic demand levels in the mid-range models are at the level of life safety performance, but in the short-range models, the seismic demand has been increased to the performance level of the collapse. so, in the mid-range models under the study, the use of buckling restrained braces with a reduced cross-sectional area to the extent of 50% of the initial cross-sectional area, will be appropriate to meet the design goals and to improve with this level of performance.
- In the studied models, where the reduction of the cross-sectional area was 25%, the amount of seismic demand was at the level of life safety performance. Therefore, the use of buckling restrained braces (with a 25% reduction in cross-sectional area) in short and mid-range models will be appropriate to meet design and improvement goals.
- Models with larger openings and with a 25% reduction in cross-sectional area have more absorbed strain energy than the rest of the models, which, compared to models with smaller openings, indicate more energy absorption in the mentioned models. Similar results have been obtained regarding the doughy energy loss of the studied different models.
- Reducing the cross-sectional area of the buckling restrained braces to 25% will result in a 12% reduction in the weight of the used materials, and as a result, will save about 10% in the required costs. Reducing the cross-sectional area to 50% will lead to a reduction in the weight of the

consumed materials to about 25%, which will save about 22% in costs. Reducing the cross-sectional area to 75% will cause The weight reduction of the materials used for the buckling restrained braces to about 38%, which will lead to save in the costs related to the buckling restrained braces to about 35%.

7. Investigating the seismic behavior of buckling restrained braces with steel casing without fillers

In a research conducted by Mr. Rezvani Sharif and Mrs. Ghafari in 2016, the seismic behavior of buckling restrained braces with steel casing without fillers was investigated. In this research, 11 buckling restrained braces and one normal brace were modeled in ABAQUS software and behavior of buckling restrained brace models under the influence of the presence of steel casing, no use of filler, the cross-sectional shape of the core of the diagonal members and the thickness of the steel casing under the effect of the same periodic loading, were checked.

- The results of the analyzes show that the energy loss capacity of the buckling restrained brace is about 5 times the energy loss capacity of the normal brace. The ability of dissipate energy and the ultimate capacity of the diagonal member section when using no fillers is reduced compared to the capacity of the section when using fillers, and the core of the diagonal members of the brace with a circular cross-section is more resistant than the two UNP and cross-sectional area.

In this study, 11 samples of buckling restrained brace and one normal brace were modeled and cyclically loaded in ABAQUS software. The results are as follows:

- The use of steel casing increases the bearing capacity of the double UNP brace to about 7%.
- The energy loss capacity in the buckling restrained brace is about 5 times of the normal convergent brace.

- In the sample with a cross section of the core and plate in the state of no filling compared to the state with mortar, because of the creation of buckling waves in the core due to the existence of a free distance between the core and the casing, the final capacity has decreased to about 50-58%.
- By calculating the area of the load-displacement diagram for cross sections and plates, in two cases of with and without filler material, it was observed that the use of filler material in the mentioned samples due to delaying the phenomenon of local buckling of the core, the ability to waste energy has increased up to 4 times.
- In the comparison of three samples with UNP, cross and circular sections, it was found that the energy loss capacity in the section with a circular core is equal to 1.12 and 1.67 respectively, compared to two UNP and cross sectional area.
- In the comparison of three samples with sections of UNP, cross and circular cores, it was found that the final capacity of the sample in the section with circular core has increased by 10% and 21%, respectively, compared to two UNP and cross sectional area.
- In buckling restrained braces without fillers, if the P_e/P_y factor is greater than 1, its increase does not have much effect on the ultimate capacity of the section.
- By choosing the appropriate shape and specifications of the core and casing for buckling restrained braces, it is possible to partially compensate for the decrease in strength due to the lack of filler material and increase the capacity of the brace.

8. An Analytical Study of Seismic Performance of a New Type of Reduced Length Buckling Restrained Brace (RLBRB) with S-shaped Core

In a research conducted by Mr. Shafaei and Tahmasabi, the seismic performance of short-length

buckling restrained brace with S-shaped core was investigated and analyzed. In this research, a new and innovative idea called a short-length buckling restrained brace with an S-shaped core has been introduced, which despite its very short length can have the same performance as the RLBRB and BRB system and at the same time act as a passive control system. Therefore, firstly, the analytical models of RLBRB and BRBs braces were validated in ABAQUS software based on the laboratory results of past researchers, and then, according to the results of the analysis, the specifications of short-length buckling restrained braces with S-shaped core were compared with RLBRB and BRB braces. The results of comparing the proposed design with conventional buckling restrained braces show that despite being smaller and lighter, these braces have the same behavior as conventional BRB braces.

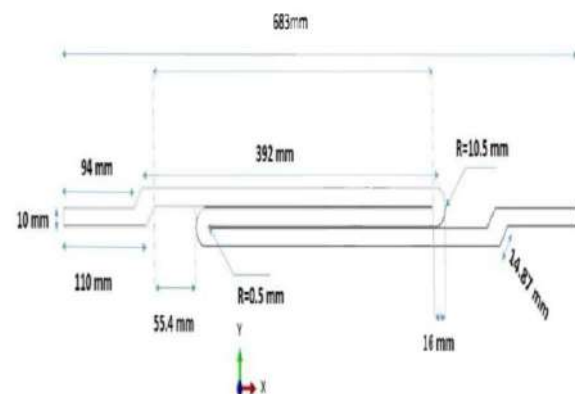


Fig.8. Details of the core of the S-shaped brace. [6]

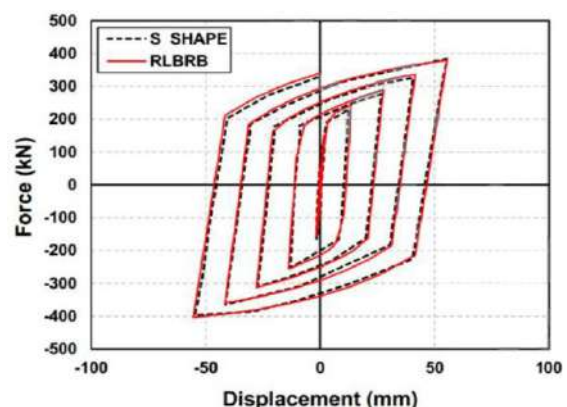


Fig.9. Comparison of hysteresis diagram of RLBRB brace and short length brace with S-shaped core. [6]

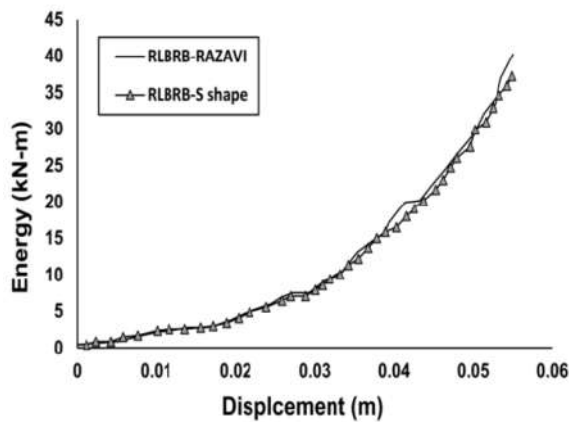


Fig.10. Comparison of cumulative energy loss of RLBRB brace and short length brace with S-shaped core. [6]

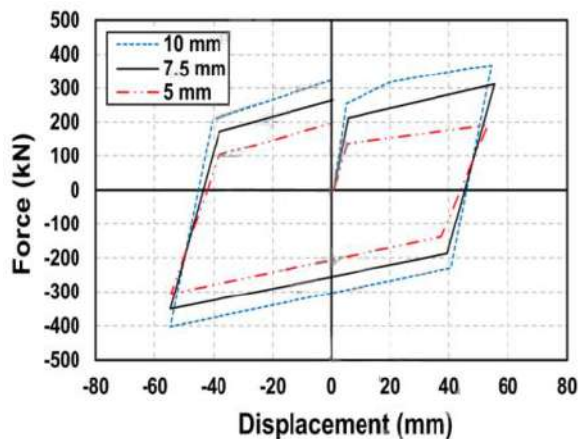


Fig.11. The effect of the core thickness on the hysteresis diagram of the short s-shaped brace. [6]

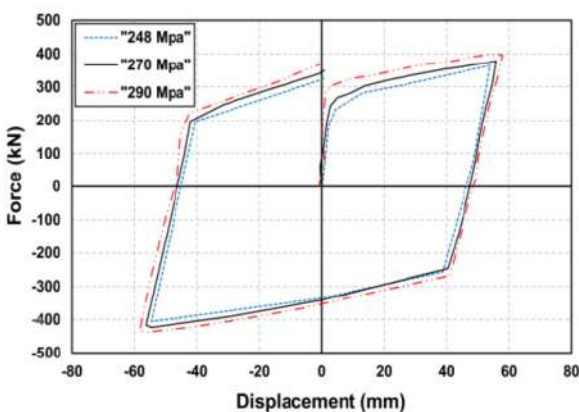


Fig.12. The effects of yield stress on the hysteresis diagram of short length s-shaped brace. [6]

In this research, a new type of short-length buckling restrained braces with an s-shaped core has been presented. The purpose of this research is to solve some of the implementation and performance problems in the common long and short buckling restrained braces. The short length brace with S-shaped core was subjected to nonlinear analysis under the effect of cyclic loading using ABAQUS software. The results of nonlinear finite element analysis show that:

The intended brace showed stable cyclic behavior without loss of strength and stiffness until the end of the ISC 341 standard loading protocol, and no overall buckling occurred in it. Due to the creation of a very small distance between the core and the casing, the local buckling was limited, which itself causes a uniform distribution of stress in the brace. Also, based on the results of the analysis, it was determined that the energy loss of the proposed brace with an S-shaped core is similar to that of common short length braces. Based on the results of this research, short-length buckling restrained braces with a S-shaped core are suggested as an alternative to conventional braces due to their lightweight and easy portability.

9. Results

- 1) Scaled nonlinear dynamic analysis has a good capability in estimating the seismic response of buildings. Therefore, this method is an efficient method when the number of records corresponding to the construction of the building is not available (such as in Iran).
- 2) The ductility factor of frames braced with buckling restrained braces is higher than other systems.
- 3) The average factor of ductility in frames with buckling restrained braces is around 5.
- 4) Frames with buckling restrained braces have higher ductility than other systems.

- 5) The average factor of behavior obtained for the braced system with buckling restrained brace is about 8.
- 6) Reducing the cross-sectional area of the buckling restrained brace has led to a reduction in the length of the yield area and the contact surface between the core and the casing, and therefore the transfer friction force to the casing has also been reduced, and the length of the buckling area has also been shortened. As a result, the steel casing of the brace can be replaced with a shorter length, which will be economical due to cost savings.
- 7) The capacity of energy loss in the buckling restrained brace is about 5 times that of the normal convergent brace.
- 8) By choosing the appropriate shape and specifications of the core and casing for the non-buckling braces, it is possible to partially compensate for the decrease in strength caused by the lack of filler material and increase the capacity of the brace.
- 9) Energy loss of short length brace with S-shaped core is similar to conventional short length braces. Short-length buckling restrained braces with an S-shaped core are recommended as an

alternative to conventional braces due to their lightweight and easy portability.

References

- [1] Sohrabi MR. Principles of writing a review article. *Pejouhandeh* 2013;18(2):52-6.
- [2] Ghodrati Amiri, Gh., Darvishan, E. and Rahgozar, F., 2014. "Evaluating the seismic behavior of steel structures with buckling restrained bracing by the scaled nonlinear dynamic analysis method". *Sharif Journal of Civil Engineering*, 30-2(1/2), pp. 13-20.
- [3] Dehghan, F. and Tasnimi, A. A., 2016. "Determination of the Parameters Influencing Behavior Factor of Buckling Restrained Braced Reinforced Concrete Frames". *Amirkabir Journal of Civil and Environmental Engineering*, 48(4), pp. 365-374.
- [4] Raissi Dehkordi, M., Foroughi, A. M. and Eghbali, M., 2017. "The effect of the yield zone length on the seismic performance of Buckling Restrained braces". *Sharif Journal of Civil Engineering*, 33-2(2/2), pp. 69-77.
- [5] Rezvani Sharif, M. and Ghafari, S., 2018. "Investigating the seismic behavior of Buckling Restrained braces with steel casing without fillers". *Sharif Journal of Civil Engineering*, 34-2(3/2), pp. 117-124.
- [6] Tahmasebi, R. and Shafaei, J., 2018. "An Analytical Study of Seismic Performance of a New Type of Reduced Length Buckling Restrained Brace (RLBRB) with S-shaped Core". *Shahrood Journal of Civil Engineering*.
- [7] Saberi, V., Saberi, H., Alipour, E. and Sadeghi, A.A., 2020. "The Effect of Material and Specifications of Link Beam Variations on the Cyclic Performance of Eccentric Buckling Restrained Brace". *Civil & Project Journal*, Second year, 2(3), pp. 34-50



fragility curves for steel moment frame with welded flange plate connection

Ali Mirzaee ^a, Mir Hamid Hosseini ^{b,*}, Mohammad Reza mansoori ^c

^a*P.h.D. Student in Structural Engineering, Department of Civil Engineering, Chalus Branch, Islamic Azad University, Chalus, Iran*

^{b,*}*Assistant Professor Civil Engineering, Science and Research Branch, Islamic Azad University, Tehran, Iran*

^c*Assistant Professor Civil Engineering, Science and Research Branch, Islamic Azad University, Tehran, Iran*

Journals-Researchers use only: Received date: 2022.07.10; revised date: 2022.08.25; accepted date: 2022.09.23

Abstract

The importance of evaluating the performance of structures against earthquakes is not hidden from anyone. It is important to have an overview of the resistance level of the structure to achieve a safe and economical design against the potential input forces. Therefore, a lot of research is always done in this area in different ways.

This article contains the method and results of the study of seismic vulnerability for WFP connection which is widely used and pre-approved connection for steel moment frames that Has been introduced in the tenth section of the Iranian building code. The purpose is to draw the fragility curve using numerical methods.

Due to the fact that this connection is pre-approved just for medium moment frames, it is necessary to check its reliability if want to use it in a special moment frame. The probability of structural damage caused by seismic force can be presented as a function of ground motion characteristics and various design parameters Using fragility curves. In this study, seven records of earthquake accelerograms were used for incremental nonlinear dynamic analysis (IDA) those most consistent with the site intended for this structure.

(DOI:<https://doi.org/10.52547/JCER.4.3.11>)

Keywords: Fragility curves, incremental nonlinear dynamic analysis, pre-validated connections

* Corresponding author. Tel.: +989123976452; e-mail: Mirhamid.hosseini@srbiau.ac.ir

1-Introduction

Earthquake is one of the natural and destructive phenomena that always threatens the safety of buildings and the lives of their inhabitants in more parts of the world. For this reason, reducing the amount of damage caused by this phenomenon at the lowest cost has always been the goal of many types of research by researchers and scientists in earthquake and structural engineering.

after the Kobe earthquake (1995) which was associated with collapse and unforeseen damage to structures and also the frequency of brittle failure of welded joints of steel moment frame buildings in the Northridge earthquake (1994), the adequacy of the design and execution processes doubted

It raised the importance of assessing the likelihood of collapse and the extent of damage to existing buildings against future earthquakes. Then Extensive research was done on the strength and ductility of steel beam-to-column joints. A wide range of these studies focused on estimating the moment-curvature relationship and determining the force capacity and deformation of joints. Steel moment resisting frames with their flexible behavior and the possibility of creating wide and large architectural spaces have many applications in the design of buildings.

The performance of the joints in these frames includes the transfer of shear force due to gravity and the transfer of flexural moment due to lateral forces between the beam and the column.

In addition, the moment-rotation behavior of moment resistance connections is a very important factor in determining the overall behavior of the frame and therefore plays an important role in the absorption and dissipation of energy due to seismic excitation. In order to facilitate and standardize the design of special and medium moment resistance frame joints, a number of joints have been introduced in a pre-approved manner in Section 10 of the Iranian code. so that there is no need for independent testing in each project.

The requirements of these joints are determined and specified in such a way that to are capable of withstanding nonlinear deformations for the purpose of controlled collapse. This goal is achieved either by weakening the beam or by strengthening the joint to form a plastic hinge in the beam area.

One of the most common pre-approved welded connections in Iranian code is the welded flange plate (WFP) connection. Section 10th of the Iranian code has limited its use to medium and ordinary moment resistance frames. This connection is the only pre-approved connection in Iran that does not exist in AISC 358 standard. The bottom and top reinforcing plates are connected to the column flange by full groove welding with full penetration and to the beam flange by corner welding. These plates are responsible for tolerating moments on the

column. Usually, the bottom plates are welded to the column in the factory. Therefore, the possibility of obtaining a groove weld with $\phi = 1$ is expected for it. But the top plate is welded to the column on the site and it is better to use a reduced factor of 0.75 or 0.85 for this weld. As a result, to ensure the required dimension and length of the weld, the top plate needs to be increased in width at the connection to the column, so, the top plate becomes a trapezoid or a cow head shape.

In summary, the process of studying the vulnerability of welded connections of steel moment frames in this article is as follows: Time history records related to the project area are selected. Records are scaled on different levels. The frame is modeled in ETABS software., Dynamic analysis of nonlinear time history is performed on the frame using earthquake records. Shears of the target columns are noted as the output of the frame analysis. The finite element model is simulated in ABAQUS software. Shear forces are applied in incremental steps to the finite element model. Maximum of time history drift for each connection in an earthquake is taken For all analyzes, with 0.1g incremental steps. Then IDA curve of connections based on maximum spectral acceleration and the connection rotation is plotted for all records.

2-background research

The production of fragility curves began in 1980 with the construction of nuclear facilities. Then, these curves were slightly developed by Kercher and Martin in 1993. These curves were computationally simple to some extent rudimentary and were prepared only experimentally with the help of engineering judgment. These curves were used to estimate the seismic damage of buildings. It can be said that after the Northridge earthquake (1994) more attention was paid to estimating the extent of structural damage. In 1994, the ATC-13 criteria for wooden structures, steel bending frames, and reinforced concrete (40 structures) were used to plot the brittle curves of structures in California. Ananus et al. Conducted further studies in 1995 based on the load distribution in the ATC and proposed a new model of the fragility curve. To date, many researchers around the world have done a lot of research on this subject.

3-Validation check

Validation in Abaqus means accurate modeling of a laboratory model in the finite element environment of Abaqus and its analysis and obtaining results similar to laboratory results.

Generally, to start these works, you choose a model similar to what you have in mind in terms of geometry, loading, etc., study the laboratory test paper of that model, and then create the model based on the Abaqus training section methods.

Therefore, by comparing the results of the tested model with the model simulated in Abaqus, the correctness of the modeling method is confirmed. In this research, the model made by Jahanbakhshi, Fanai, and Rezaian was used as a reference sample to verify the accuracy of finite element modeling results with a laboratory model. The desired model consists of a connection node and half of the beam span and two halves of the column height. And the loading was carried out in accordance with the regulations of SAC. Figure 1 shows the proper matching of the load-displacement diagrams of the laboratory sample and the finite elements

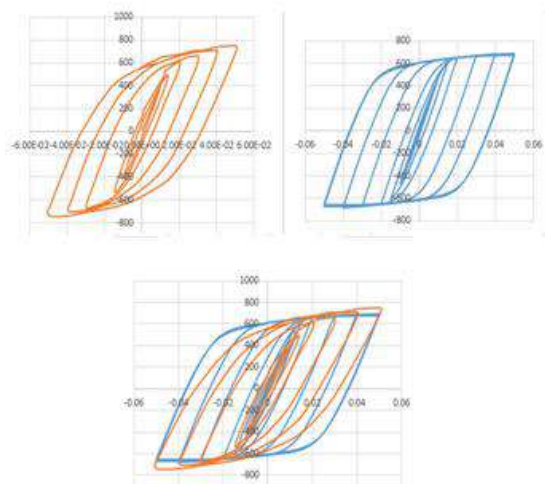


Figure 1 - Matching the hysteresis curve resulting from the modeling with the hysteresis curve of the article

4-Research Methods

According to the studies conducted after the Northridge and Kobe earthquakes, it can be said that velocity in near-field earthquakes and acceleration in far-field earthquakes are the controlling parameters. here the records of far-field earthquakes have been used because, in this research, the acceleration criterion has been studied.

Choosing the right accelerograms is one of the most important steps in nonlinear analysis. Because the nonlinear responses of the structure are highly dependent on the selected acceleration. For this reason, the selected earthquakes should have the same characteristics as the probable earthquake at the site under study. These specifications include the following: Magnitude, Distance, Fault Mechanism, Soil/Rock Type and Directivity.

These records were selected from the record tables suggested by FEMA365 in research work And downloaded from the "peer ground motion database". The names of these earthquakes can be seen in the table.

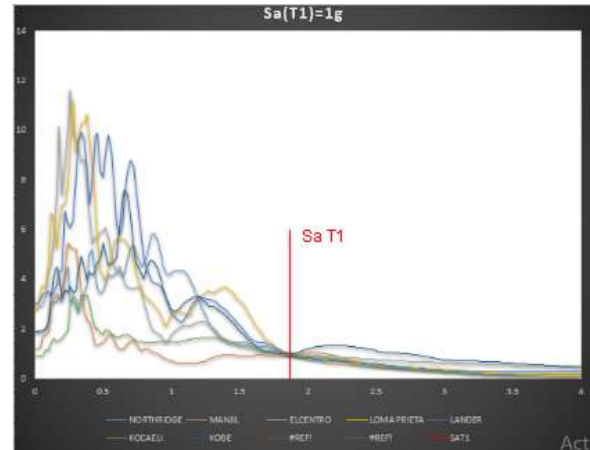


Figure 2- Earthquake spectra in the scaled mode of spectral acceleration equal to one

In this research, the spectral acceleration in the first period of structure $S_a(T_1)$ is used as the intensity parameter and incremental dynamic analysis (IDA) is done. The response spectra of selected earthquakes are scaled in terms of spectral acceleration. For this purpose, the value of the spectrum at the period of the structure (T_1) is specified and by dividing the whole spectrum by this number, the amount of spectral acceleration at the time of the main period of the structure will be equal to one. Given that an incremental step for incremental dynamic analysis is selected equal to 0.1, it is easy to multiply the existing range by 0.1 to 0.9 to obtain the spectra required for the analysis. This procedure was performed for each of the 7 selected earthquakes. So in the end, there were 70 earthquakes that can use to do the analysis.

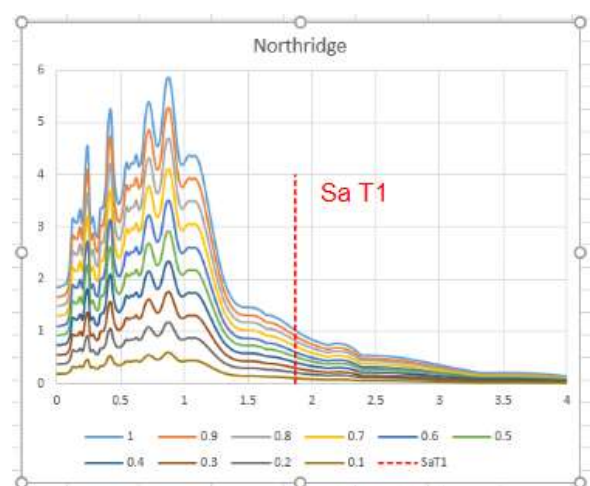


Figure 3-Northridge earthquake spectra in scale mode with step 0.1

5-Structural model

For modeling the frame in Etbas software, all the rules and restrictions related to the design of beams, columns, and pre-approved connections have been observed in accordance with the tenth section of the Iranian building code. Gravitational loads on the structure are in accordance with the sixth section of Iranian building code. Lateral loads on the structure are calculated according to the Iranian 2800 standard. The project site has been assumed as a high-level seismic risk area. The soil is assumed as type two soil. The structure is residential.

The research variables are shear and displacement, which are examined and measured as follows: The shear force is taken from Etbas software under nonlinear dynamic analysis. The shear force extracted from Etbas software is applied to the finite element model in Abaqus finite element software. The maximum displacement is specified at the top point of the column in Abaqus software.

The structural model is a 2D 10-story bending frame with three spans of different lengths. Beams and a middle column on the second floor and a beam and a corner column on the eighth floor will be used for design. In this structure, box sections for columns and I-shaped sections for beams are used. In order to investigate the ductility of the types of connections expressed in each step, after performing the analysis on the 2D frame, the amount of shear is extracted from the software by applying the selected records.

6-Incremental dynamic analysis (IDA)

Incremental dynamic analysis (IDA) is a parametric analysis method That is used in several different forms to estimate more thoroughly structural performance under seismic loads.

It involves subjecting a structural model to one (or more) ground motion record(s), each scaled to multiple levels of intensity, thus producing one (or more) curve(s) of response parameterized versus intensity level. [1]

magnitude of the earthquakes measured by IM. IDA curves are plotted to plot damage magnitude (DM) against one or more severity measures (IM) based on two or more dimensions independent of IM. In this method, the maximum amount of acceleration is increasingly scaled from a very small value, during which the response of the structure is elastic and gradually increases until we reach a limit point after the surrender. In this case, the maximum values of the base shear versus the maximum displacement after each analysis are plotted, which is called the pushover dynamic diagram or IDA push curve.

6-1--Drawing IDA curves

After obtaining the change history at the Up Column point, the most displacement is picked, so there is maximum displacement per spectral acceleration; By obtaining the maximum displacement rate can draw the IDA curve. The

following tables show the maximum rate of change in the column's up-point for the spectral acceleration of each model of connection, respectively.

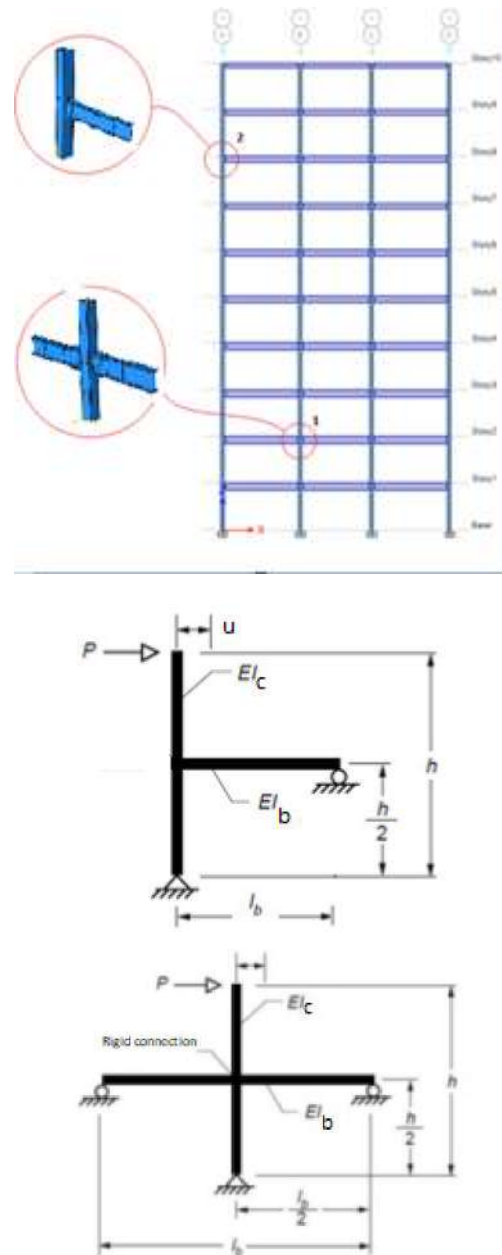


Figure 4: Force application point and boundary conditions

6-2-Building performance levels

The level of performance of the whole building is defined in terms of the level of performance of its structural and non-structural components. The different levels of performance of the building are: Operational Performance (OP), Immediate Occupancy Performance (IO), Life Safety (LS) and Collapse Prevention Performance (CP).

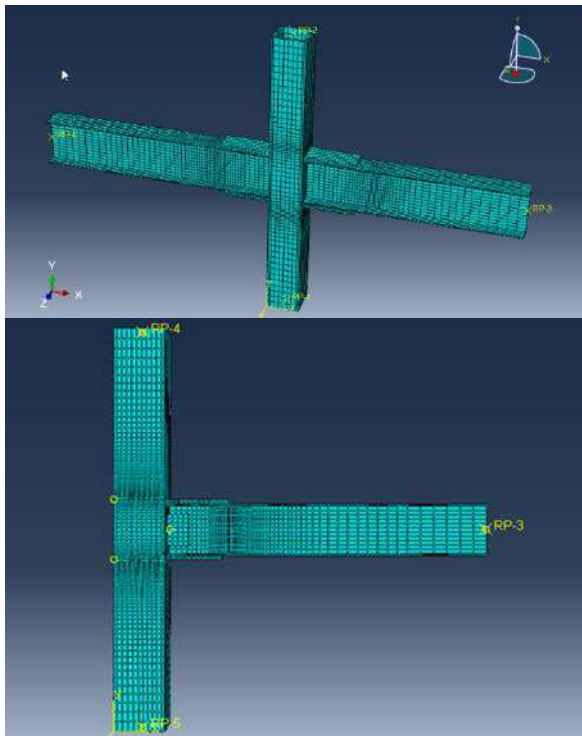


Figure 5: Meshed Model in ABAQUS

6-3-Failure curve and its requirements

here the Numerical concepts and standard deviations are described to investigate and plot pre-confirmed connection failure curves.

Definition of arithmetic criterion, variance and standard criterion deviation:

In mathematics and statistics, the arithmetic mean is the sum of a collection of numbers divided by the count of numbers in the collection.

$$\bar{x} = \frac{1}{n} \sum_{i=1}^n X_i = \frac{1}{n} (x_1 + \dots + x_n)$$

Which is used for a random example with n members of a statistical community. The mean of the main population n is generally defined as follows:

$$\mu_x = \frac{\sum_{i=1}^n X_i}{N}$$

Where N is the total number of members in the community.

In probability theory and statistics, variance is the expectation of the squared deviation of a random variable from its population mean or sample mean. Variance is a measure of dispersion, meaning it is a measure of how far a set of numbers is spread out from their average value.

$$\sigma_x^2 = \frac{\sum (X_i - \mu_x)^2}{N}$$

The above expression is known as variance and is denoted by the symbol σ^2

In statistics, the standard deviation is a measure of the amount of variation or dispersion of a set of values. A low standard deviation indicates that the values tend to be close to the mean (also called the expected value) of the set, while a high standard deviation indicates that the values are spread out over a wider range.

The standard deviation is defined as follows.

$$\sigma_x = \sqrt{\frac{\sum_{i=1}^n (X_i - \mu_x)^2}{N}}$$

6-4-Function of normal log distribution

A random variable x has logarithmic normal distribution functions (or normal log distribution), if the variable $Y = \ln(X)$ has a normal distribution, then the probability density function of variable X is as follows:

$$f_x(x) = \frac{1}{\sqrt{2\pi\xi_x}} \exp\left[-\frac{1}{2}\left(\frac{\ln x - \lambda}{\xi}\right)^2\right]$$

$$0 \leq x \leq \infty \quad (11)$$

Where $\xi = \sqrt{\text{var}(\ln(x))}$ and $\lambda = \ln(X)$, which are the mean and standard deviation of the variable $\ln(X)$, are the distribution parameters, respectively.

6-5-LOGNORM.DIST function in Excel software

The Excel software calculates the value of the normal logarithm distribution density or the cumulative probability based on the normal logarithm utilization function (the LOGNORM.DIST function) or a value of the distribution (x value) and the normal logarithm distribution service (mean and standard deviation). The shape of this function is as follows: LOGNORM.DIST (value, mean, standard deviation, cumulative or normal)

Here the parameters of this function are described:

Value: is a number that we want to get the cumulative probability value based on the normal logarithm distribution

Mean: The first parameter of the logarithm distribution is normal (a numerical value).

Standard deviation: The second parameter of the normal logarithm distribution, which is equal to the standard deviation (a numerical value).

Cumulative or Normal: A logical value for determining whether you want the cumulative probability value to be obtained or only the density value to be calculated. If this input is set to zero (False), the density value, and if it is set to one (True), then the cumulative probability value will be calculated.

After that, the results that the function returns are:

The LOGNORM.DIST function returns the value of the normal logarithm distribution density or the cumulative probability for the normal logarithm distribution function with defined parameters

The data tables obtained from the normal log distribution of IDA curves are given below.

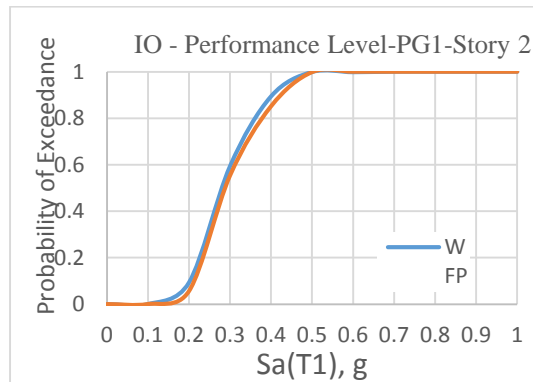


Figure 6- Comparison of fragility curves of WFP and WUF-W junctions in story 2

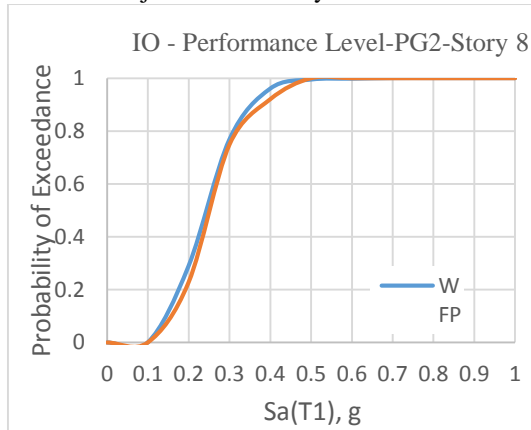


Figure 7- Comparison of fragility curves of WFP and WUF-W junctions in floor 2

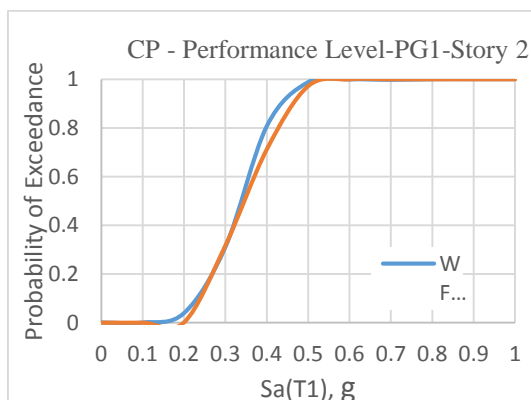


Figure 8- Comparison of fragility curves of WFP and WUF-W junctions in floor 8

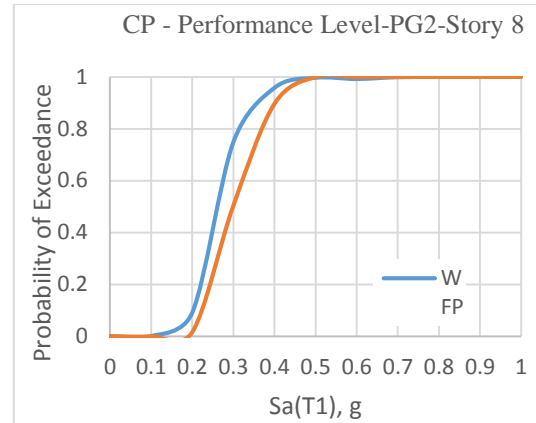


Figure 9- Comparison of fragility curves of WFP and WUF-W junctions in floor 8

7-Discussion on the accuracy of IDA results

The most important issue in assessing the accuracy of this method is if the average value of responses (or any other statistical value) obtained using the Earthquake Scale Records can be the same as the actual values obtained from real earthquakes?

Although a large amount of research is devoted to this, it is difficult to answer this question due to the limitation of seismic records that have equal IM.

In general, the answer to this question depends a lot on the structure, DM and IM values, and the population of records we use. However, the answers obtained from this method can be a piece of good evidence for the correctness of the hypotheses. For example, a comparison of studies that considered the value of the DM parameter for rotation, and the value of the IM parameter to be PGA or $S_a(T1)$, shows that $S_a(T1)$ shows less scatter in the range of DM values and it can be concluded that the spectral acceleration parameter in the first mode of the structure ($S_a(T1)$) is a more appropriate parameter. The data tables from the normal log distribution of IDA curves are presented in table 1 to 4.

8-The overall result

Fragility curves are undoubtedly one of the most useful and widely used tools for determining the probability of earthquake vulnerability. In this study, seismic fragility curves for two joints of the second and eighth floors of a steel bending frame were investigated.

Failure criteria were selected based on two levels of " Immediate Occupancy Performance " (IO) and " life safety " (LS).

The curves were calculated and plotted based on the effect of 7 different earthquake records that are as similar as possible to the type of soil and other

Table 1 - IDA curve normal log distribution data for IO performance level of second floor

Data for IO Performance Level story2

Earthquake	SaT1 (Sorted)	ln(SaT1)	Sa(T1)	ln(SaT1)	$\varphi\left(\frac{X - \mu}{\sigma}\right)$
kobe	0.241	-1.422958	0.1	-2.3026	4.83743E-15
Kocaeli	0.289	-1.241329	0.2	-1.6094	0.000924313
Landers	0.323	-1.130103	0.3	-1.204	0.342665781
elcentro	0.362	-1.016111	0.4	-0.9163	0.935290187
loma	0.321	-1.136314	0.5	-0.6931	0.998680358
Manjil	0.319	-1.142564	0.6	-0.5108	0.999988039
Northridge	0.401	-0.913794	0.7	-0.3567	0.999999926
			0.8	-0.2231	1
			0.9	-0.1054	1
			1.0	0	1
Mean (μ)	-1.143310449				
Standard Deviation (σ)	0.149710194				

Table 2 - IDA curve normal log distribution data for CP performance level of second floor

Data for CP Performance Level story2

Earthquake	SaT1 (Sorted)	ln(SaT1)	Sa(T1)	ln(SaT1)	$\varphi\left(\frac{X - \mu}{\sigma}\right)$
kobe	0.33	-1.108663	0.1	-2.3026	1.4925E-32
Kocaeli	0.442	-0.816445	0.2	-1.6094	3.83354E-10
Landers	0.419	-0.869884	0.3	-1.204	0.002295434
elcentro	0.491	-0.711311	0.4	-0.9163	0.315330686
loma	0.412	-0.886732	0.5	-0.6931	0.91065795
Manjil	0.414	-0.881889	0.6	-0.5108	0.997719115
Northridge	0.483	-0.727739	0.7	-0.3567	0.999979128
			0.8	-0.2231	0.999999895
			0.9	-0.1054	1
			1.0	0	1
Mean (μ)	-0.857523342				
Standard Deviation (σ)	0.122229322				

Table 3- IDA curve normal log distribution data for IO performance level of 8th floor

Data for IO Performance Level story8

Earthquake	SaT1 (Sorted)	ln(SaT1)	Sa(T1)	ln(SaT1)	$\varphi\left(\frac{X - \mu}{\sigma}\right)$
kobe	0.33	-1.108663	0.1	-2.3026	0.000768753
Kocaeli	0.21	-1.560648	0.2	-1.6094	0.239852029
Landers	0.23	-1.469676	0.3	-1.204	0.768116112
elcentro	0.22	-1.514128	0.4	-0.9163	0.960280676
loma	0.412	-0.886732	0.5	-0.6931	0.994553784
Manjil	0.17	-1.771957	0.6	-0.5108	0.99929693
Northridge	0.21	-1.560648	0.7	-0.3567	0.999908222
			0.8	-0.2231	0.999987494
			0.9	-0.1054	0.999998196
			1.0	0	0.999999723
Mean (μ)	-1.410350085				
Standard Deviation (σ)	0.281683429				

Table 4- IDA curve normal log distribution data for CP performance level of 8th floor

Data for CP Performance Level story8					
Earthquake	SaT1 (Sorted)	ln(SaT1)	Sa(T1)	ln(SaT1)	$\varphi\left(\frac{X-\mu}{\sigma}\right)$
kobe	0.23	-1.469676	0.1	-2.3026	5.44781E-06
Kocaeli	0.271	-1.305636	0.2	-1.6094	0.090535124
Landers	0.245	-1.406497	0.3	-1.204	0.674788776
elcentro	0.275	-1.290984	0.4	-0.9163	0.957615054
loma	0.23	-1.469676	0.5	-0.6931	0.996626883
Manjil	0.46	-0.776529	0.6	-0.5108	0.999779542
Northridge	0.24	-1.427116	0.7	-0.3567	0.999986361
			0.8	-0.2231	0.999999144
			0.9	-0.1054	0.999999944
			1.0	0	0.999999996
Mean (μ)	-1.306587828				
Standard Deviation (σ)	0.226435557				

conditions of the site. These curves can be used to estimate the overall seismic vulnerability.

The results of IDA analysis in this study and similar studies indicate that this method of analysis can be very effective in evaluating the seismic performance of structures. Therefore, despite the limitations of this method, it seems to can replace the usual and approximate methods such as load analysis due to its strengths. This method considers the behavior of materials nonlinearly and has a dynamic nature. Therefore, compared to static methods such as linear static analysis (pushover) and other linear methods such as dynamic linear spectral analysis can be the most accurate method of estimating structural behavior.

The following results can be deduced from the obtained failure curves :The presented curves show that in general, the more the curves move to the left, it means that the probability of fragility increases.

That is, the probability of the structure passing the low failure state occurs at lower spectral acceleration values . And occurs in moderate, extensive, and general failure modes at higher values of spectral acceleration, respectively .In other words, with increasing Sa, fragility increases.

By increasing the intensity parameter or seismic requirement, the probability of exceeding a certain limit state will be higher. In other words, according to fragility curves, in earthquakes with different return periods, the probability of exceeding a certain limit state of failure for a structure or

part It determined. Therefore, fragility curves are undoubtedly one of the most useful and widely used tools to determine the probability of earthquake vulnerability.

In this paper, two joints of steel bending frames were investigated, and brittleness curves were prepared for both joints. According to the fragility diagram of the joints, the results showed that the behavior of the two joints is somewhat similar. Both connections performed satisfactorily Also, the performance of the WUF-W connection was somewhat better than the WFP connection. In some cases, especially at high seismic intensities, the WFP connection shows a slight increase in damage. And it has less reliability than connecting a steel bending frame using a WUF-W connection.

9-Acknowledgments

finally, this part is the only section in that I can say what my heart wants to say. I appreciate my wife for revival me. my eyes became able to see after The first time I saw her.

References

- [1]. IRANIAN CODE FOR SEISMIC RESISTANT DESIGN OF BUILDINGS (Standard No. 2800).
- [2]. "Iranian National Building Code, Part 10, Steel Structure Design", Tehran (Iran): Ministry of Housing and Urban Development; (2013).

- [3]. "Iranian National Building Code, Part 6, Structural loading", Tehran (Iran): Ministry of Housing and Urban Development; (2019)
- [3]. Federal Emergency Management Agency (FEMA), "Prestandard and Commentary for the Seismic Rehabilitation of Buildings", (FEMA 356), Washington, DC, (2000).
- [4]. Management and Planning Organization "Instructions for Seismic Improvement of Buildings", Issue No. 36
- [5]. Office of Codification and Promotion of National Building Regulations "(1398) National Building Regulations Topic Six: Loads on the building".
- [6]. Office of Codification and Promotion of National Building Regulations "(2013) National Building Regulations Topic 10: Design and Execution of Steel Buildings".
- [7]. Regulations for designing buildings against standard earthquake 2800 (fourth edition).
- [8]. Rezaei, Ali Asghar and Hosseini, Mirhamid, 1398, Probabilistic comparison of End Plate flange connection performance with IDA incremental dynamic analysis, 6th National Conference on Applied Research in Civil Engineering, Architecture and Urban Management and 5th Specialized Exhibition of Mass Builders in Tehran, Tehran
- ""
- [9]. Evaluation of incremental nonlinear dynamic analysis (IDA) method in studying the seismic behavior of structures - Ahmad Niknam – Hamidreza Ahmadi - Navideh Mahdavi. The First National Conference on Improvement and Rehabilitation of Urban Tissues in the Adjacent to Active Fault, Tabriz, 2012
- [10]. Seyed Mozaffar Davari- Reza Rahgozar- Comparison of incremental nonlinear dynamic analysis and incremental nonlinear static analysis in seismic analysis of a steel frame - The Second International Conference on Research in Science and Technology - Turkey - Istanbul - 2015
- [11]. Earthquake Engineering and Structural. Dynamics. 2002; 31:491–514 (DOI: 10.1002/eqe.141)
- [12]. Incremental dynamic analysis Dimitrios Vamvatsikos and C. Allin Cornell*; † Department of Civil and Environmental Engineering; Stanford University; CA 94305-4020; U.S.A



Numerical evaluation of fracture behavior of split concrete beams reinforced with steel sheet

Lobat Hosseinzadeh  a,*

P.h.D. Student in Structural Engineering, Department of Civil Engineering, Chalus Branch, Islamic Azad University, Chalus, Iran

Journals-Researchers use only: Received date: 2022.07.15; revised date: 2022.08.29; accepted date: 2022.09.28

Abstract

Since the parameters affecting the strengthening of cracked beams and their failure behavior after strengthening are very important, this research is devoted to the numerical investigation of the failure behavior of cracked concrete beams reinforced with steel sheet. The investigated beams have an initial crack in the middle of the span and are reinforced with a steel layer under the beam. Using the finite element method and non-linear static analysis, the bearing capacity of the samples, the growth and opening of the crack opening have been evaluated. First, in order to evaluate the accuracy of the modeling, the results obtained with the data obtained from the existing laboratory work were compared, and after ensuring the correctness of the modeling, the effect of changing various parameters, including sheet thickness, mechanical characteristics of concrete, initial crack length, was investigated. The results show that the load-opening diagrams of the crack openings have two maximum load points, the first and second maximum points increase with the increase of concrete strength and sheet thickness, and due to the increase in the initial crack length, the first maximum point decreases, while the maximum point The second remains almost unchanged. (DOI:<https://doi.org/10.52547/JCER.4.3.20>)

Keywords: cracked concrete beam, steel sheet, crack opening, nonlinear finite element method;

*Corresponding author. Tel.: +989113927782; e-mail: lobi_h@yahoo.com

1. Introduction

Nowadays, strengthening of concrete structures with the help of FRP is used as a new method in the field of strengthening. Using FRP for strengthening compared to traditional methods has advantages such as increased strength and hardness, light weight, good corrosion resistance, low thickness, easy to carry and install. After installing the sheet to the concrete beam, the response of the structure, including ductility, strength and failure parameters, is different compared to the behavior of the unreinforced structure. Therefore, experimental tests, analytical and numerical methods are necessary to predict the behavior of structures after retrofitting. The presence of cracks in structures is inevitable, so regardless of its effect, the safety of the structure may be compromised. On the other hand, crack growth due to repeated loading that is generally applied to structures is an issue that, without considering it in the design, it is possible to significantly reduce the useful life of the structure. In recent years, a number of researchers investigated the nature of the separation mechanism between FRP sheet and concrete by using fracture mechanics and determining the obtained energy [1-4]. Taljesten [5] presented a linear equation to calculate the bearing capacity of reinforced concrete with FRP sheet. under tensile axial load and based on it, the maximum load and ultimate load is a function of fracture energy (GF), modulus of elasticity and thickness of FRP sheet

Yashiza et al. [6, 7] succeeded in determining the fracture energy and the stress-strain relationship by conducting a one-way shear test on reinforced concrete samples with FRP sheets. Wu and Yen [8] studied the behavior of cracking and failure due to separation of reinforced concrete beams reinforced with FRP sheets. By performing finite element analysis and by examining different types of separation development during the interaction between concrete and FRP sheet and crack distribution in concrete, they found that the properties of adhesive and concrete have the greatest effect on the types of separation development and crack distribution. Also, the bond strength, fracture energy of adhesive layer, tensile strength and fracture energy of concrete were fully investigated and the effect of these parameters on concrete cracking

behavior, structural bearing capacity and types of separation were studied. In order to postpone the separation of the sheet from the concrete surface, different solutions have been presented and investigated experimentally and by simulation. Shahbaz Panahi et al [9], by presenting a numerical method, investigated the shear strengthening of reinforced concrete beams using FRP sheets. They focused their studies on determining the length of FRP failure zone, energy release rate and crack propagation path. The results show that the failure mode in the existing model and the control beam (without reinforcement) is due to diagonal shear cracks. Also, the failure mode of the reinforced sample in the laboratory is concrete shear rupture and sheet separation, while the failure of the corresponding modeled sample is It is due to the rupture of the steel sheet in the opening of the cut Considering that FRP sheets can delay the crack development and reduce the width of the crack opening in concrete, many researches [12-10] analytically presented relationships to predict the bearing capacity of cracked reinforced concrete beams. In this regard, Wu and Davids [13], considering the non-slip between concrete and FRP sheet, found that the crack growth stops when its length increases to a certain value. A number of researchers investigated the resistance of concrete samples reinforced with FRP sheets to peeling by performing peeling tests. They considered the effect of different types of FRP sheet and glue, the way of preparing the concrete surface and the strength of concrete on the flaking of the samples and by determining the fracture energy by analytical method, they found that the fracture energy of the contact surface of concrete and FRP sheet and the hardness of the sheets in the flaking of the samples should be be considered[14] High stresses may cause cracks to form near the contact surface of concrete and FRP, and if the necessary energy is provided for their expansion, these cracks will progress. Recently, nonlinear fracture mechanics models have been presented [17-15], and the results of one-way shear tests were used to determine the fracture parameters. In any case, due to the difference between the failure mode of the reinforced beams and the one-way cut test samples, these methods cannot be used to determine the exact failure parameters.

Katz [18], in order to investigate the stress transfer mechanism between reinforced concrete beams and

steel sheets and GFRP, 36 beams with integrated concrete cross-section and with a weak concrete top, which indicates the damaged surface of the concrete, were built and recorded and analyzed the spread of strains in concrete and FRP layers. has done. The results show that the presence of a weak concrete layer on the surface does not have much effect on the bearing capacity, and the type of FRP has the greatest effect on the bearing capacity, and in general, it can be said that increasing the strength of the concrete core of the samples with a weak top layer of concrete increases the bearing capacity. .

Many researches have been done on the behavior of FRP-reinforced concrete members, but what is important is the proper amount and manner of strengthening the members after cracking with FRP sheets. In this context, Wu et al.[19] investigated the fracture of concrete beam reinforced with FRP sheet using analytical method and compared the results with what was obtained from the three-point bending test of reinforced beams. They concluded that in the early stages of loading, the P-CMOD relationship is linear, but after the first crack, it is nonlinear. In fact, after the amount of load reaches its first maximum value, it decreases and the crack opening opens. In the continuation of loading, due to the combined performance of concrete and FRP sheet, the amount of load increases until it reaches its second maximum point. They attribute the fluctuations observed in the crack opening load-distension curves to the different adhesion conditions between the FRP sheet and concrete at different points.

Achinta and Borgon [20] used the concepts of fracture mechanics based on total energy balance to determine the load under which the FRP sheet separates from the concrete beam. They found that the only important and effective parameter is the fracture energy of the contact surface of concrete and FRP sheet, and the development of separation occurred in the concrete area between the sheet and tensile steel bars, and also the presence of steel bars prevents the development of the fracture area. The results show that the deviation of the FRP sheet force from the crack opening causes tensile stresses in the crack opening and for this reason the crack starts to progress.

Mohammadi et al.[21] performed a one-way shear test to investigate the effective parameters on the interaction zone of concrete and steel sheet and also investigated the effect of boundary conditions on the

resistance of the interaction zone with the help of numerical analysis. In another study [22], by combining the adhesive crack method and the damaged concrete model, they simulated the behavior of FRP reinforced concrete beams using the advanced finite element method. In order to verify the results of the modeling, they also investigated the behavior of these beams in a laboratory. By studying how the stress spreads in the location of the main cracks, they investigated the separation of the sheet from the concrete surface in samples with a variable crack position relative to the middle of the opening and found that the separation of the sheet from the tip of the diagonal cracks and near the main bending-shear cracks where the ratio of anchor- The cut is high, it begins.

As mentioned earlier, most of the studies have been done in laboratory and analytical form around beams reinforced with FRP sheets. By using the finite element method, it is possible to make a more complete investigation about the behavior of the structures that have become resistant after cracking. Due to the high costs of laboratory research, it is appropriate to use the finite element method to more accurately estimate the behavior of these structures. The main goal of the current research is numerical modeling of concrete beams with initial crack reinforced with steel sheet using the finite element method. In this research, more details about the modeling of the samples have been discussed, including how to model the glue, which has rarely been considered in previous studies. Also, by comparing the results of modeling and laboratory results done by other researchers and ensuring the accuracy of the modeling, the parameters affecting the failure behavior of these beams after strengthening were evaluated with the help of numerical method.

2- Numerical modeling

In order to numerically analyze the concrete beams with initial crack reinforced by steel sheet, using the finite element method and ABAQUS software, a model of the laboratory sample that was implemented and tested under static load by Wu et al. [19] has been prepared and after comparing the results of the numerical model of this research and the aforementioned laboratory results and ensuring the correctness of the numerical model, the results are presented for other numerical analysis modes.

• Laboratory sample of reinforced steel beam with initial crack

In 2010 [19], ææ et al. analyzed the behavior of concrete beams with primary cracks reinforced by a layer of steel sheet under the beam analytically, numerically and experimentally. Figure 1 shows the characteristics of the beam with initial crack under three-point bending, where (b) beam width, (h) beam height, (2L) span length, (a₀) initial crack length, (h_a) adhesive thickness, (h_p) steel sheet thickness, (b_p) sheet width, (P) The applied load (2L_d) is the length of the area of the sheet that is not connected to the concrete to prevent diagonal cracking during loading.

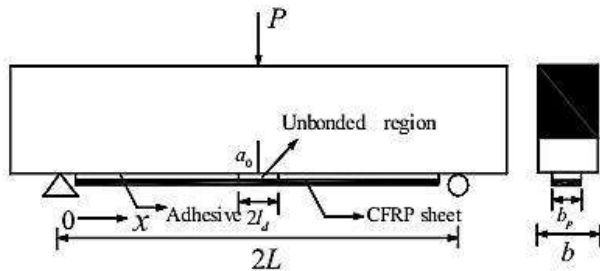


Figure 1: Concrete beam with primary crack and [19] steel sheet.

The beams were made in three groups with different heights. For the bending failure direction of the samples, the ratio of the length of the opening to the height of beam 4 is selected, the width and the ratio of the length of the initial crack to the height of the samples (a_0/h) are constant and equal to 0.3 and 150 mm, respectively. While the height is variable and three heights of 200, 250 and 300 mm have been selected. Based on the results of the tests, the mechanical characteristics of the concrete used are according to Table 1 and the characteristics of the steel sheet are also according to Table 2.

Table 1: Mechanical properties of used concrete [19].

Tensile strength (MPa)	Modulus of rupture (MPa)	Modulus of elasticity (GPa)	Poisson's ratio
28.50	23.3	45.29	248.0

The settings required to measure the bearing capacity and the crack opening of the samples under the three-point bending test are shown in Figure 2.

Table 2: Geometrical and mechanical characteristics of [steel] sheet

Sheet type	thickness (mm)	Modulus of elasticity (GPa)	Tensile strength (MPa)	Ultimate strain
CFRP	167.0	240	3916	0017.0



Figure 2: Laboratory settings for loading and recording sample data [19].

• Numerical modeling of slotted beam reinforced with steel sheet

Abaqus software version 14.6 was used to investigate the fracture behavior of the beams and the initial crack growth in the samples using the finite element method. Solid and shell elements were used in 3D modeling of concrete beam and XFEM method was chosen for crack modeling according to material properties. The criterion for crack opening is the maximum stress, so that the crack expands when the maximum stress exceeds the tensile strength of concrete

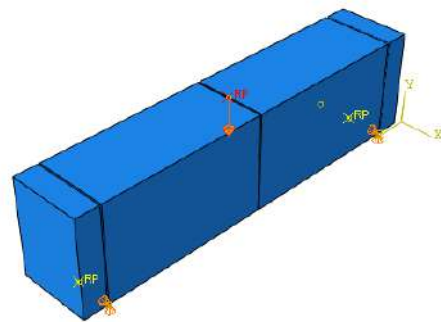


Figure 4: Beam model with initial crack and support conditions

For proper meshing, the results obtained from the analysis of the simulated samples in the software and the corresponding laboratory samples were compared with each other and by observing the convergence of the responses based on the sensitivity analysis, the size and density of the elements were selected. Also, according to Figure 5, the size of the mesh is smaller and larger in the insensitive areas due to the sensitivity of the elements to the crack growth around it.

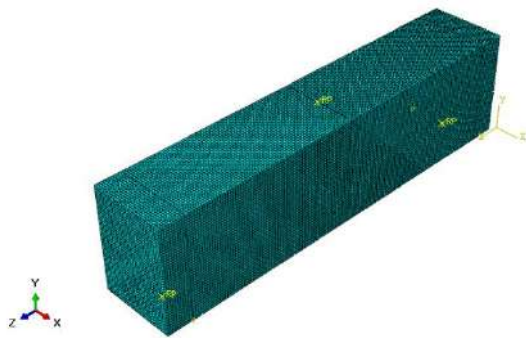


Figure 5: Finite element model meshing

3- Comparison of laboratory results and numerical analysis

The investigated beams consist of three parts: concrete, glue and steel sheet. Since the resistance of each section has an effect on the mode of failure and the rate of crack development, four stages can be considered in loading until the final failure. At first, the slip between the concrete and the sheet is insignificant, and with the application of force, the sheet is stretched in the middle of the opening and a crack develops. In this stage, separation did not occur and simultaneously with the progress of the crack, the load reaches the initial maximum point (P1max). In the next stage, while the microcracks develop and the width of the crack also increases, the bearing capacity decreases. Then in the third stage, with opening the opening of the crack, tensile stresses are added in the steel sheet and at this time the effect of the sheet affects the bearing capacity and causes the load to reach the second maximum point (P2max). Finally, the concentration of shear stresses in the vicinity of the middle of the opening along with the development of a vertical crack, Horizontal micro-cracks also increased on the common surface of concrete and sheet, leading to the separation of the sheet from the concrete and finally, the complete failure of the sample.

Wu et al. [19] numerically investigated this process and obtained the load-displacement diagrams of the crack opening. In Figure 6-A, B, and C, the P-CMOD diagram obtained from the experimental and numerical results [19], for beams with a height of 200, 250, and 300 mm, respectively, is compared with the results obtained in the present study using Abaqus software. As can be seen, the process of changes in the diagrams obtained based on numerical and laboratory methods are similar. So that at first the load changed linearly in relation to the opening of the crack opening and after the development of the crack, the behavior became non-linear, after reaching the P1max point, the bearing capacity decreased and again due to the presence of the steel sheet, the capacity increased until it reached the P2max point. Although the amount of load reduction in the laboratory is lower than the corresponding value obtained from the modeling, what is more important is the increase in capacity due to the presence of the sheet, because in the transition between the primary and secondary maximum points, the stress transfer takes place between the concrete and the sheet.

According to the results of the difference between P1max and P2max obtained from the laboratory, numerical and modeling results in this research, it is less than ten percent. The fluctuations in the graph obtained from the laboratory investigation can also be attributed to the non-uniformity of the conditions of sticking the sheet to the concrete surface along the span of the beam. The rupture of the tested samples happened due to the separation of the sheet from the concrete surface and the development of the crack [19]. In this way, the separation of the sheet started from the vicinity of the initial crack and with the progress of the crack, it moves towards the support. In figure 7-a and b, the failure mode of the laboratory sample is shown.

According to Figure 7, it can be expected that the maximum stresses in the sheet occur near the crack. In the numerical example, it can be seen that the maximum shear stresses in the steel sheet occurred near the middle of the opening, which caused the separation of the sheet from this area, and the amount of stress decreases with the distance from the initial crack location. Figure 8 shows the connection of steel sheet to concrete beam. According to the investigations, there is a relatively good agreement between the numerical and laboratory models in

different aspects. Therefore, it is possible to trust the results of numerical analyzes with the help of finite elements regarding the modeling of concrete, glue and steel sheet.

4- Parametric studies

After ensuring the validity of the numerical modeling using the finite element method, parametric analyzes have been performed for the steel plate reinforced

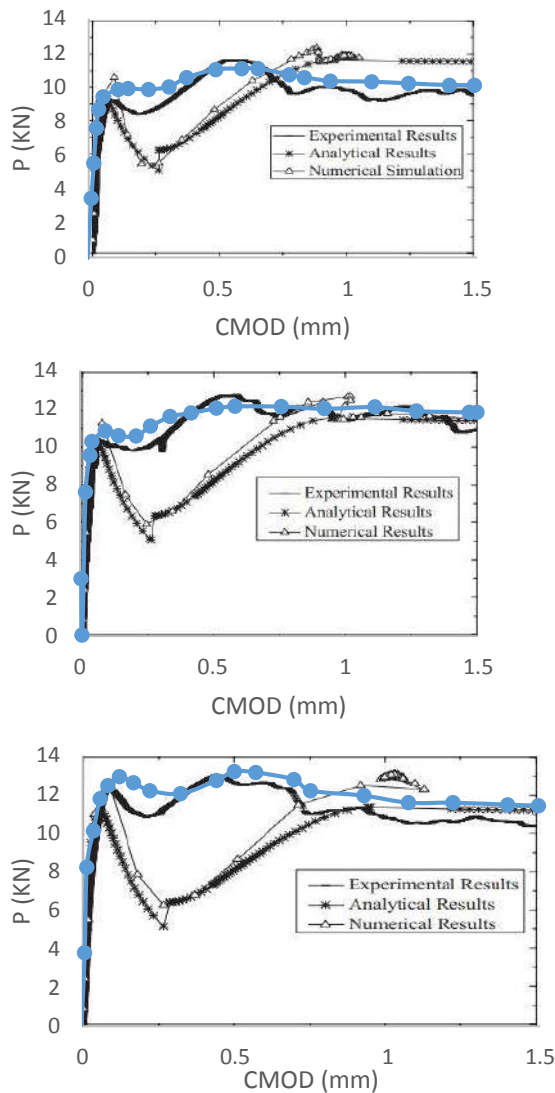
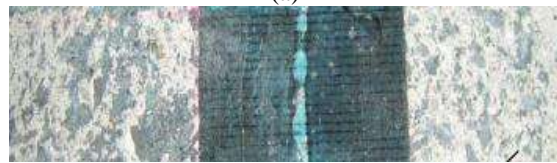


Figure 6: Comparison of P-CMOD diagrams of reference [19] and Abaqus: a) mm200h=, b) mm250h=c) mm=300h



(a)



(b)

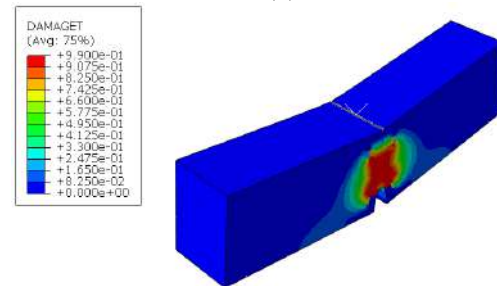


Figure 7: The method of failure of the laboratory sample a) Beam failure

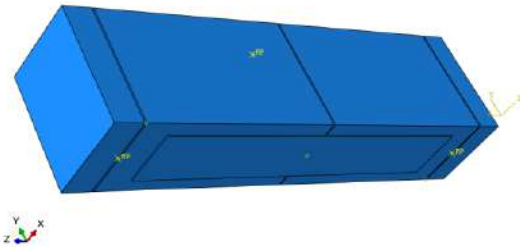


Figure 8: Connecting steel sheet to concrete beam

split beam by changing the mechanical properties of concrete, the thickness of the steel plate, the ratio of the initial crack length to the beam height, and the adhesive strength. In all analyses, the type of elements and the method of modeling are the same as those considered in the validation section

- The effect of changing the mechanical properties of concrete

In order to investigate the effect of changing the compressive strength of concrete on the fracture behavior of steel-reinforced beams, the geometric and mechanical characteristics of the sheet have been selected according to Table 2. By changing the compressive strength of concrete, other mechanical properties will also change.

This diagram is determined based on the results of the uniaxial compression test of concrete. For concrete under pressure, three areas of the diagram are introduced. The first part of the diagram is assumed to be elastic up to the corresponding limit stress. The amount of this stress is considered equal [4]. where is the compressive strength of concrete. Strain is equal to stress. Young's modulus is also calculated based on [4] and Poisson's ratio is considered equal. The second part of the diagram, which has a parabolic shape, starts from the point with the limit stress and continues until reaching the highest compressive strength of concrete. This part of the diagram is determined by the equation (1):

$$\sigma_c = \left(\frac{kn - n^2}{1 + (k - 2)n} \right) f_{ck} \quad (1)$$

$$\varepsilon_{c1} = 0.0022 \quad k = 1.1 E_{cm} \times \frac{\varepsilon_{c1}}{f_{ck}} \quad n = \frac{\varepsilon_c}{\varepsilon_{c1}} \quad (2)$$

where is the modulus of elasticity of concrete.

The third part of the stress-strain curve is the descending part of the graph from to, where the reduction factor is considered equal to 0.85. The final strain of concrete ε_{cu} at rupture $r f_c$ is equal to 0.01 stress.

The load-opening diagram of the crack opening for three cases of concrete with a resistance of 55, 45, and 35 MPa is presented in Figure 11.

According to the above figure, it can be seen that with the increase of concrete strength, the primary and secondary maximum points increase. The rate of increase for the initial maximum point of the sample with 55 MPa resistance compared to the sample with 35 MPa resistance is equal to 14% and for the second maximum point of the said samples is equal to 1.2%. This increase can be justified considering that the bond stress in the damaged area around the crack

(FPZ) as well as the shear strength in the contact surface of concrete and sheet according to equation (1) are directly proportional to the tensile strength of concrete.

Since the maximum shear stress in the steel sheet occurs around the crack, according to Figure 12, the strain of the elements is also higher in this area and

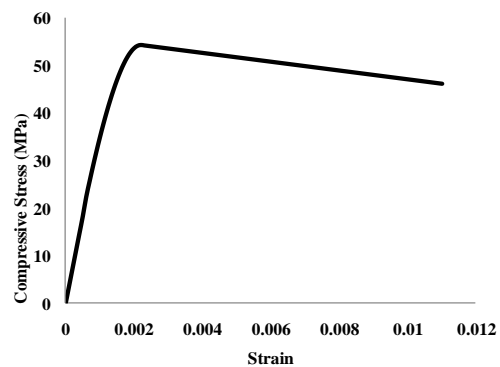


Figure 9 - Tensile stress-strain curve for concrete with a compressive strength of 55 MPa

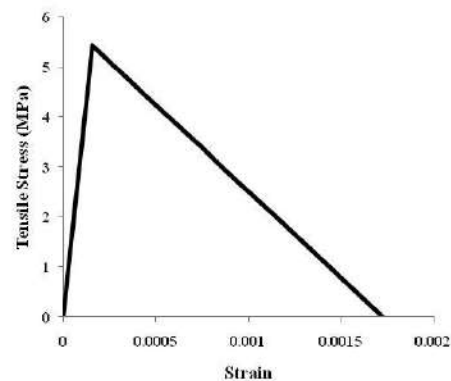


Figure 10 - Stress-strain curve for concrete with a compressive strength of 55 MPa

Table 3: Mechanical properties of concrete in numerical analysis.

pushing resistance (MPa)	Modulus of elasticity (MPa)
35	28465
45	30951
55	33442

gradually decreases as they move away from the crack.

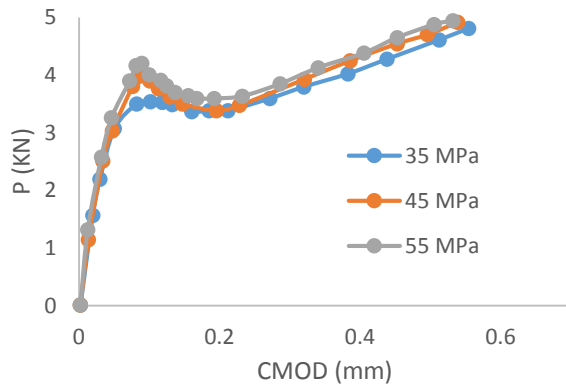


Figure 11: Load-strain diagram of crack opening for beams with resistance of 35, 45 and 55 MPa.

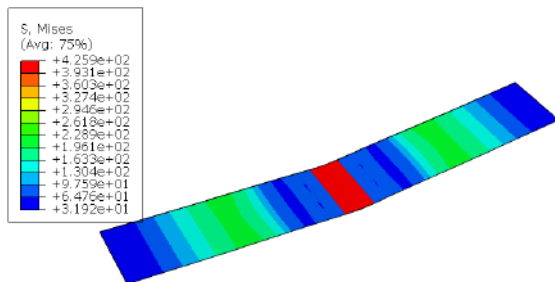


Figure 12: Stress distribution in steel sheet

- The effect of changing the thickness of the steel sheet compared to CFRP

Since the geometry of the steel sheet can be one of the influencing factors on the fracture behavior of concrete beams, the effect of changing the thickness of the sheet is investigated in this section. In this study, the geometric characteristics of the beam are fixed, the characteristic strength of concrete is 40 MPa, the crack length is 100 mm, and with other parameters remaining constant, the sheet thickness is 1.0, 15.0, and 2.0 mm. The load-displacement diagram of the crack opening is according to Figure 12.

The primary and secondary maximum load points in the diagram increase with the increase of sheet thickness. Because a sheet with a greater thickness

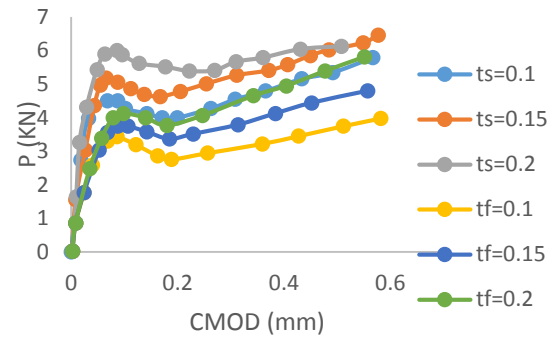


Figure 12: Load-expansion diagram of crack opening for variable thickness of CFRP sheet and steel sheet

can withstand a greater tensile force, and with an increase in thickness from 1.0 to 2.0, the primary maximum point will increase by 35% and the secondary by 19%. Therefore, it can be said that the second maximum load is more sensitive to the sheet thickness. The changes of stress along the length of the sheet with the change of its thickness are shown in Figure 13. Also, the use of steel sheet compared to CFRP sheet has shown higher initial hardness and more resistance by about 30% compared to samples with similar thickness in CFRP sheet.

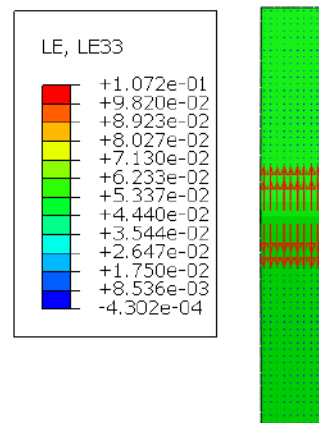


Figure 13: Strain changes along the length of the steel sheet

According to the above figure, it can be seen that in the length of the sheet which is connected to the concrete and their performance is integrated, the strains in the middle part have the highest values and by moving towards the two ends, the strains show almost zero.

• The effect of changing the initial crack length

In order to investigate the effect of the length of the initial crack on how the beam breaks as well as its bearing capacity, other parameters were considered constant for three crack lengths of 80, 100, and 120 mm. The characteristic strength of concrete is 40 MPa and the specifications of the sheet are also according to table 2. The changes in the bearing capacity of the samples in relation to the opening of the crack opening are shown in Figure 14.

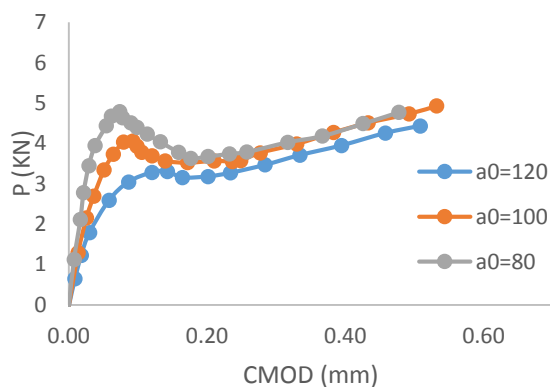


Figure 14: Load-discharge diagram of crack opening for variable initial crack length

Based on table 5, it can be seen that the reduction of the bearing capacity of the beam by changing the length of the crack from 80 to 120 mm is about 30%.

Table 5- Maximum bearing capacity of samples with different crack lengths

Thickness of steel sheet(mm)	P1max (kN)	P2max (kN)
80	3.3	4.4
100	4.05	4.93
120	4.78	4.78

It can be seen from Figure 14 that with the increase of the crack length, the primary maximum load decreases and the secondary maximum load remains almost unchanged. The reason for this behavior can

be the reduction of the bearing capacity of the beam due to the increase in the length of the crack. Because the first maximum point in the load-opening diagram of the crack opening is related to concrete failure due to crack development and the second maximum point is due to steel tensile force.

5- Conclusion

In this research, the behavior of concrete beams with primary crack reinforced with steel sheet was investigated by changing the effective parameters using the finite element method, and the following results were obtained:

- The comparison of numerical and experimental results shows that the numerical modeling of the behavior of cracked beams reinforced with steel plate by the finite element method has a good accuracy.
- Rupture of the samples occurs by separating the steel sheet from the place of the crack, and its development towards the end of the sheet simultaneously with the progress of the crack.
- According to the relationship between the characteristic strength of concrete and its other mechanical properties, with the increase of the compressive strength and then the tensile strength, the bearing capacity of the samples increases.
- By increasing the thickness of the sheet, the bearing capacity and tensile stress of the steel sheet increase in the area connected to the concrete, and the amount of stress decreases around the crack.
- Changing the length of the initial crack has a significant effect on the initial maximum load, and with the increase of the length of the crack, the load-carrying capacity is significantly reduced.

- In general, according to the obtained results, it can be seen that the length of the primary crack is the most effective factor on the primary and secondary maximum load in the load-opening diagrams of the crack opening.

References

- [1]. Wu, Z.S., and Yoshizawa, H. (1999). "Analytical/Experimental Study on Composite

Behavior in Strengthening Structures with Bonded Carbon Fiber Sheets". *Reinf Plast Compos*, Vol. 18(2), pp. 1131-55.

[2] Yuan, H., and Wu, Z.S. (2000). "Energy Release Rates for Interfacial Crack in Laminated structures". *Struct Mech*

Earthquake Eng, JSCE, Vol. 17(1), pp. 19-31

[3]. Wu, Z.S., Yuan, H., and Niu, H.D. (2002). "Stress Transfer and Fracture Propagation in different Kinds of Adhesive

Joints". *Eng Mech, ASCE*, Vol. 128(5), pp. 562-73

[4]. Achintha, M., and Burgoyne, C. (2013). "Fracture Energy of the Concrete- FRP Interface in Strengthened Beams". *Eng*

Fracture Mech, Vol. 110, pp. 38-51

[5]. Taljsten, B. (1996). "Strengthening of Concrete Prisms using the Plate-Debonding Technique". *Int J Fract*, Vol. 81, pp.253-66.

[6]. Yoshizawa, H., Wu, Z.S., Yuan, H., and Kanakubo, T. (2000). "Study on FRP-Concrete Interface Bond Performance".

Mater Concrete Struct Pavements, JSCE, Vol. 49(662), pp. 105-19

[7] Wu, Z.S., Yuan, H., Yoshizawa, H., and Kanakubo, T. (2001). "Experimental/Analytical Study on Interfacial Fracture

Energy and Fracture Propagation along FRP-Concrete Interface". *ACI International Special Publication*, Vol. 201, pp. 133-52.

[8] Wu, Z., and Yin, J. (2003). "Fracture Behavior of FRP-Strengthened Concrete Structures", *Fracture Mechanics*, Vol. 0, pp. 1339-1355.

[9] Shahbazpanahi, S., Abdullah, A., Kamgar, A., and Farzadnia, N. (2015). "Fracture Mechanic Modeling of Fiber Reinforced Polymer Shear-Strengthened Reinforced Concrete Beam". *Composites: Part B*, Vol. 68, pp. 113-120.

[10] Baky, H., Ebead, U., and Neale, K. (2007). "Flexural and Interfacial Behavior of FRP-Strengthened Reinforced Concrete Beams". *J. Compos. Constr.*, Vol. 11(6), pp. 629-639.

[11] Wang, J., and Zhang, C. (2008). "Nonlinear Fracture Mechanics of Flexural-Shear Crack Induced Debonding of FRP Strengthened Concrete Beams". *International Journal of Solids and Structures*. Vol. 45, pp. 2916-2936

[12] Zheng, J. J., Dai, J. G., and Fan, X. L. (2016). "Fracture Analysis of FRP-Plated Notched Concrete Beams Subjected to Three-Point Bending". *Eng*

Mech, ASCE, Vol. 142(3).

[13] Wu, Z.J., and Davies, J.M. (2003). "Mechanical Analysis of a Cracked Beam Reinforced with an External FRP Plate". *Compos Struct*, Vol. 62(2), pp. 139-143.

[14] Wu, Z., Yuan, H., Kojima, Y., and Ahmed, E. (2005). "Experimental and Analytical Studies on Peeling and Spalling Resistance of Unidirectional FRP Sheets Bonded to Concrete". *Composites Science and Technology*, Vol. 65, pp. 1088-1097.

[15] Wang, J., and Zhang C. (2008). "Nonlinear Fracture Mechanics of Flexural-Shear Crack Induced Debonding of FRP Strengthened Concrete Beams". *Int J Solids Struct*, Vol. 45(2), pp. 2916-36.

[16] Lu, X. Z., Teng, J. G., Ye, L. P., and Jiang, J. (2007). "Intermediate Crack Debonding in FRP-Strengthened RC Beams:

FE Analysis and Strength Model". *Compos. Constr.*, Vol. 112, pp. 161-174.

[17] Mohammadi, T., Wan, B., and Dai, J. G. (2011). "Modeling of Concrete Interface Subjected to Coupled Pull-Out and Push off actions". *ACI Spec. Publ.*, Vol. 275(19), pp. 1-18.

[18] Katz, A. (2007). "Stress Transfer between FRP Laminates and Concrete through Deteriorated Concrete Surfaces". *Compos Constr*, Vol. 11(4), pp. 410-418.

[19] Wu, Z., Yang, S., Hu, X., Zheng, J., Fan, X., and Shan, J. (2010). "Analytical Solution for Fracture Analysis of Sheet-Strengthened Cracked Concrete Beams". *Eng. Mech.*, Vol. 136(10), pp. 1202-1219.

[20] Achintha, M., and Burgoyne, C. (2013). "Fracture Energy of the Concrete-FRP Interface in Strengthened Beams".

Engineering Fracture Mechanics, Vol. 110, pp. 38-51.

Mohammadi, T., & Wan, B. (2015). "Sensitivity Analysis of Stress State and Bond Strength of Fiber-Reinforced Polymer/Concrete Interface to Boundary Conditions in Single Shear Pull-Out Test". *Advances in Mechanical Engineering*, 7(5), 1687814015585419.

Mohammadi, T., Wan, B., Harries, K. A., and Sweriduk, M. E. (2015). "Bond Behavior of FRP-Concrete in Presence of Intermediate Crack Debonding Failure". *Journal of Composites For Construction*, Vol. 21(5).

[23] Lu, X. Z., Teng, J. G., Ye, L. P., and Jiang, J.

(2005). "Bond-Slip Models for FRP Sheets/Plates Bonded to Concrete".
Eng. Struct., Vol. 276, pp. 920-937.
CEB-FIP, (Fédération Internationale de la Précontrainte). (1993). CEB-FIP model cod 1990, Thomas Telford, Lausanne, Switzerland.



Experimental study of compressive strength, permeability and impact testing in geopolymer concrete based on Blast furnace slag

Mohammadhossein Mansourghanaei^{a*}, Morteza Biklaryan^b

^{a,b}Department of Civil Engineering, Chalous Branch, Islamic Azad University, Chalous, Iran

Article History: Received date 12 July 2022; revised date 9 September 2022; 23 September 2022

Abstract

Cement production has always been associated with environmental challenges due to carbon dioxide emissions. On the other hand, cement production is an energy-intensive process and leads to the consumption of abundant fossil fuels. In order to solve this problem, the production of geopolymer concrete is on the agenda. The researchers decided to reduce the negative effects of cement production and have superior properties than ordinary concrete. In the current study, slag-based geopolymer concrete was used with 0-2% polyolefin fibers and 0-8% nano-silica to improve its structure. After curing the specimens under dry conditions at a temperature of 60°C in an oven, they were subjected to compress strength, tensile strength and Drop weight hammer tests to evaluate their mechanical properties, as well as Permeability test to assess their durability. tests were performed at 7 and 90 days of age at ambient temperature (20°C). The addition of nano-silica enhanced the whole properties of the slag-based geopolymer concrete. Increasing the curing age improved the results of all tests. The results of all tests in geopolymer concrete showed the superiority of the results over conventional concrete. At the 28-day curing age, the addition of up to 8% nanosilica to the geopolymer concrete composition improved the compressive strength test results by 19.01%, water permeability by up to 35% and impact strength by up to 36.36%. Addition of up to 2% of polyolefin fibers in the composition of geopolymer concrete resulted in a 28.95% decrease in compressive strength but a 20% improvement in water permeability and an 8.26-fold increase in impact strength. In the following, by conducting the SEM test, a microstructure investigation was carried out on the concrete samples. In addition to their overlapping with each other, the results indicate the geopolymer concrete superiority over the regular concrete. Besides, it demonstrated the positive influence of nano-silica addition on the concert microstructure. © 2017 Journals-Researchers. All rights reserved. (DOI:<https://doi.org/10.52547/JCER.4.3.31>)

Keywords : Geopolymer Concrete; Polyolefin Fibers; Nano Silica; Blast Furnace Slag; Scanning Electron Microscope (SEM).

* Corresponding author. Tel.: +98-912-171-2070 ; E-mail: Mhm.ghanaei@iauc.ac.ir

1. Introduction

Today, the reduction of mineral and fossil resources and the need for concrete with high mechanical properties and durability, led scientists to think about finding a suitable material to replace cement in concrete. On the other hand, annual cement production emits high volumes of toxic CO₂ gas into the atmosphere. Research shows that cement plants are responsible for emitting about 5% of the total CO₂ into the Earth's atmosphere [1]. In order to solve these problems, the replacement of cement with pozzolanic materials containing abundant aluminosilicate materials that can create good adhesion in concrete was considered, the final product of this process is called geopolymer concrete. Geopolymer is a name coined by Davidovits [2]. The amount of CO₂ produced in the geopolymer process is much less than the cement production process [3]. Geopolymer cements are a group of alkali-activated materials exhibiting superior engineering properties compared to Portland cements [4]. Geopolymer is characterized by high polymerization materials with aluminosilicate structure, which is mainly composed of three cross-linked unit dimensions, including SiQ₄(2Al) and SiQ₄(3A) [5]. In Portland cement, C-S-H gel consists of silicone and geopolymer groups of materials with high polymerization and Aluminosilicate structure [6]. Replacing cement with these pozzolans reduces environmental pollution, improves the mechanical properties of concrete, and lowers the considerable need for cement [7,8]. In alkaline concrete, instead of cement, geopolymeric materials containing abundant aluminosilicate materials and alkaline solutions are used, which combine together in a chemical process called geopolymerization to produce hydrated gels with high adhesion and filling properties. These gels play an important role in improving the mechanical properties and durability of concrete by affecting the microstructure of concrete. The structure of concrete can be evaluated in microstructural and macrostructural dimensions. The macrostructural dimension consists of large components visible to the naked eye, which is divided into two phases of aggregate and cement paste, but in the microstructural dimension most components must be observed by electron microscope (SEM) devices. In the microstructure dimension (in the geopolymerization process), C-S-H crystals and the second generation of

crystals formed from calcium hydroxide (Ca(OH)₂) and ettringite gel (C-A-S-H) begin to fill in the gaps in the ettringite and calcium hydroxide network (called Portelite). And with this operation, the density, hardness and strength of the interfacial transfer area (ITZ) of concrete increases. Comparing the concrete containing regular Portland cement with geopolymer concrete, McNulty [9] asserted that the geopolymer concretes have higher compressive strength. Granulated Blast Furnace Slag (GBFS) is among the environmental materials. Using this material instead of cement can improve concrete resistance and decrease the increasing demand for its usage in concrete [10,11]. Ground granulated blast-furnace slag (GGBFS) has latent hydraulic properties that could be activated using suitable activators [12]. The activation of blast-furnace slag with alkaline liquids (e.g., NaOH or water glass) to produce alkali-activated slag cement has been studied during the past few decades [4]. In addition to positively affecting the mechanical properties, the presence of silica particles in the geopolymer concrete accelerates the geopolymer reaction, reducing the compound alkalinity [13]. The influence of the nano-silica in improving the strength can be attributed to the following multi-stage mechanism that improves the concrete's microstructures and thus, increases the mechanical properties.

1. The rise in the pozzolanic reaction [13]. The presence of nano-silica in the geopolymer concrete accelerates the pozzolanic reaction.

2. The filling effect of nano-silica particles [14,15]. First, the distribution of nano-silica particles besides the other concrete particles results in a denser matrix. Second, the nano-silica's reaction in the geopolymerization procedure produces a larger amount of aluminosilicate gel, along with the reaction products of the main materials. The reaction by-product is likely to deposit in the structure of the existing pores. The rise in SiO₂ increases the matrix density [16]. Therefore, the filling effect of Nano-silica is improved by the particle packing, and the by-product produces a denser matrix, reducing the porosity and increasing the strength.

3. It acts as a nucleus [17,18]. In the C-S-H gel structure, nanoparticles can act as a nucleus and form strong bonds with the C-S particles of the gel. Thus, during the hydration, the products' stability increases, and the durability and mechanical products are expected to improve.

Improved compressive strength have been reported with the use of nano-silica in geopolymer concrete [19]. nanoparticles prevented the reduction in the geopolymer strength [13]. And In the sample containing nano-silica, very few fine cracks are observed, in which nano-silica acts as a filler to fill the spaces inside the hardened microstructure skeleton of the geopolymer paste and increase its compaction [20,21]. The nano-silica addition to the geopolymer concrete increases the geopolymerization reaction. In this case, more amorphous geopolymer gel is created in the matrices. This issue, in turn, indicates that the nano-silica particles prevent the resistance decline of geopolymer concrete[13]. The simultaneous evaluation of nano-silica and steel fibers in geopolymer concrete has indicated a good relationship between them [22,23]. Preventing the connection of pores and bonding the flow channels in the concrete, the polyolefin fibers strengthen it and avoid its spalling [24]. According to the studies, using macroplastic fibers for concrete improvement instead of metal mesh and fibers has captured researchers' attention; the concrete-related industries widely use polyolefin-based fibers[25]. In an investigation on the effect of polyolefin fibers with different diameters and lengths in geopolymer concretes, it was revealed that the proper use of fibers increases the compressive strength, and impact energy, and reduces water absorption. Besides, adding fibers decreases the compressive strength[26]. The addition of fibers reduces the compressive strength [27]. The reason for the reduction in the compressive strength of specimens containing polyolefin fibers can be the micro internal defects in the geopolymer matrix caused by the additional fibers [28]. But in an investigation on the effect of polyolefin fibers with different diameters and lengths in geopolymer concretes, it was revealed that the proper use of fibers increases the compressive strength and impact energy, and reduces water absorption. Besides, adding fibers decreases the compressive strength[26]. the effectiveness of fibers when facing impact loads is extremely more than nano-silica in concrete samples. Besides, by the addition of polyolefin fibers to geopolymer concrete, concrete has become more flexible. This behavior is also observed by other fibers in the investigations conducted by other researchers[25,29,30].

In this laboratory study, increasing the mechanical properties and durability of slag geopolymer concrete containing nanosilica and polyolefin fibers is one of the innovative goals. On the other hand, according to the research of others, helping the healthy environment by reducing CO₂ emissions from conventional cement production, is another goal in this research.

2. Experimental program

2.1 Materials

In this experimental study, the Portland cement type II with a 2.35 g/cm³ of specific weight according to standard En 197-1 and the Blast Furnace Slag was used in powder form with the density of 2.45 g/cm³ according to ASTM C989/C989M standard. The chemical properties of these materials are indicated in Table 1. The nano-silica particles made up of 99.5% SiO₂ with an average diameter in the range of 15 to 25 nm were used. Crimped polyolefin fibers according to ASTM D7508/D7508M standard, 30 mm in length, were also used, whose physical properties are shown in Fig. 1. The used fine aggregates were natural clean sand with a fineness modulus of 2.95 and a density of 2.75 g/cm³, and the coarse aggregates were crushed gravel with a maximum size of 19 mm and a density of 2.65 g/cm³ according to the requirements of the ASTM-C33. In this study, the geopolymer concrete curing has been performed at 60 °C according to the geopolymer concrete standards extracted from prestigious articles in this field.

Table1. Chemical compositions of materials

Component	Slag (%)	Portland cement type II (%)
SiO ₂ (%)	29.2	21.3
Al ₂ O ₃ (%)	19.4	4.7
Fe ₂ O ₃ (%)	5.8	4.3
CaO (%)	38.6	62.7
MgO (%)	2.8	2.1
SO ₃ (%)	2.6	2
K ₂ O (%)	0.1	0.65
Na ₂ O (%)	0.2	0.18
TiO ₂ (%)	0.6	-
Free Cao	-	1.12
Blaine (cm ² /g)	2200	3200
LOI (%)	0.3	1.84


Tensile Strength (N/mm ²)	>500	
Length (mm)	30	
Diameter (mm)	0.8	
Elasticity Modulus (G. Pa)	>11	
Bulk Density(g/cm ³)	2400	

Fig. 1. Physical properties of the polyolefin fibers

2.2 Mix design

For accurate investigation, six mixture designs were considered, according to ACI 211.1-89 standard. The first sample included a regular concrete containing Portland cement where the water to cement ratio has considered to be constantly 0.45. Five other samples include geopolymers concrete with different nano-silica and polyolefin fibers. The geopolymer concrete samples are generally categorized into two groups: the first group lacks polyolefin fibers with the nano-silica amount of 0-8%. The second group contains 8% of nano-silica, where the polyolefin fibers are used in these designs in the form of 1 and 2 percent. In order to achieve the

same performance in each mixture design and obtain a slump of about 20 ± 100 mm, we have used normal polycarboxylate-based superplasticizers. Besides, 202.5 kg/m^3 of the alkaline solution is used in this case. The used alkaline solution is a combination of NaOH and Na_2SiO_3 with the weight ratio of 2.5, utilized with the mixture specific weight of 1483 kg/m^3 and the concentration of 12 M. The conducted studies indicate that due to the significant level of C-S-H formation when utilizing Na_2SiO_3 , using a combination of NaOH and Na_2SiO_3 increases the compressive strength compared to single employment of CaOH [31]. The samples mixture design is indicated in Table 2.

Table 2. Details of the mix designs

Mix ID	Cement	Slag	Water	Alkaline solution	Nano silica	Coarse aggregates	Fine aggregates	polyolefin fibers	Super plasticizer	
	(Kg/m ³)									
1	OC	450	0	202.5	0	0	1000	761	0	6.75
2	GPCNS0PO0	0	450	0	202.5	0	1000	816	0	6.75
3	GPCNS4PO0	0	432	0	202.5	18	1000	767	0	7.8
4	GPCNS8PO0	0	414	0	202.5	36	1000	718	0	8.3
5	GPCNS8PO1	0	432	0	202.5	36	1000	672	24	8.6
6	GPCNS8PO2	0	432	0	202.5	36	1000	646	48	9

2.3 Test Methods

After fabricating the samples, for better curing and increasing the resistance properties, the samples were placed in an oven at 80°C with a thermal rate of 4.4°C/min for 48 h. In this study, the compressive strength tests were performed on 10-cm^3 cubic specimens based on BS EN 12390. The concrete's resistance to dynamic loads (impacts) was measured

using the drop weight hammer test according to the report by the ACI 544-2R committee. This test was conducted with repeating impacts on disks with a diameter of 15 cm and a height of 63.5 cm. According to EN 12390-8, the water permeability tests were performed on $150 \times 150 \times 150\text{-mm}^3$ cubic specimens with a water pressure of $50 \pm 500 \text{ kPa}$ on a circular area with a diameter of 75 mm on one of the

surfaces for 72 hours. The permeability coefficient is calculated as the following [32]:

$$K = \frac{e^2 v}{2ht} (m/s) \quad \text{Eq. 1}$$

where e is the penetration depth (m), v is the volume fraction of concrete, h is the hydraulic length of concrete, and t is the duration it is under water pressure.

3. Results and discussion

3.1 Results of the compressive strength test

The results of the compressive strength test are shown in Figure 2. Figure 3 shows a concrete sample undergoing compressive strength test. Following these results, it is observed that increasing the curing age in the samples has improved the results up to 48.89% in ordinary concrete and 21.78% in geopolymer concrete. In each processing period, the maximum amount of results is related to the GC-NS8PO0 scheme. Addition of nanosilica to geopolymer concrete designs has improved the results. At the 90-day curing age (as the best performance), the addition of 8% nanosilica improved the compressive strength by 21.94%. Nanosilica particles due to their high filling and adhesion properties have been able to help produce a large volume of hydrated gels in the composition of concrete, these gels in combination with other materials and by creating a proper bond have increased the strength of concrete. The minimum compressive strength obtained at the age of 90 days at 62.43 M.Pa belongs to the OC-NS0PO0 design and the maximum at 82.96 M.Pa belongs to the GP-NS8PO0 design. Addition of polyolefin fibers to the composition of geopolymer concrete has reduced the compressive strength. In this regard, at the curing age of 90 days, adding 2% of fibers to concrete has caused a 22.49% decrease in compressive strength. The reason for the reduction in the compressive strength of specimens containing polyolefin fibers can be the micro internal defects in the geopolymer matrix caused by the additional fibers [28].

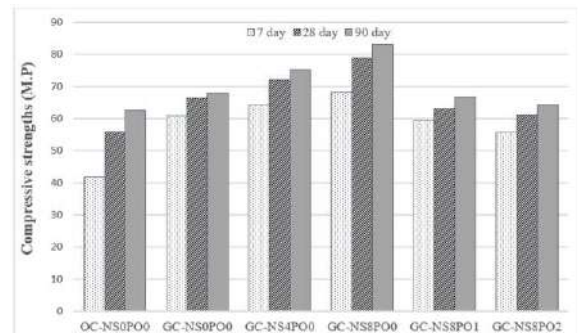


Fig. 2. The compressive strengths of the specimens



Fig. 3. Concrete sample in compressive strength test

3.2 Results of the impact test

The required fracture energy and adsorbed energy in concrete specimens are shown in Figure 4 based on the results of the hammer impact test at a working age of 90 days at a temperature of 20%. The lowest (427.43 J) and highest (3439.76 J) energy required for failure of concrete samples belong to OC-NS0PO0 design and GC-NS8PO2 design, which has a difference of 7.04 times. Addition of 8% nanosilica to 58.33% and addition of 2% polyolefin fibers to the geopolymer concrete design up to 3.44 times improved the fracture energy. The lowest (223.89 J) and highest (2829.15 J) amount of energy absorbed in concrete samples belong to the design, which has a difference of 11.63 times. Addition of polyolefin fibers to the geopolymer concrete design had a significant effect on improving the impact test results. The fibers prevent them from spreading by bridging the cracks. Preventing the connection of pores and bonding the flow channels in the concrete, the polyolefin fibers strengthen it and avoid its

spalling [24]. Figure 5 shows the concrete sample after the impact strength test.

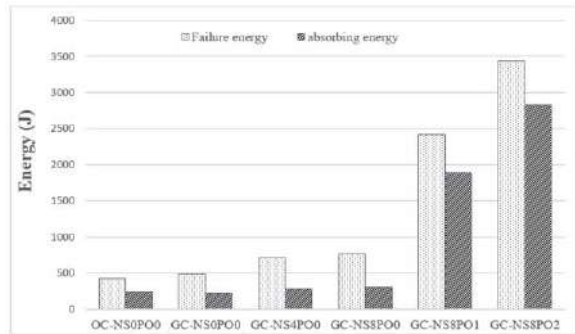


Fig. 4. The impact of the specimens



Fig. 5. Pattern of fracture of specimens in impact test

3.3 Results of the water permeability test

The results of water permeability test in concrete samples at 7, 28 and 90 days of curing age are shown in Figure 6. Figure 7 shows a concrete sample measuring the amount of water absorption in a concrete sample. Increasing the curing age has reduced the water penetration coefficient by 36.1% in ordinary concrete and up to 84.35% in geopolymer concrete samples. At the processing age of 90 days (as the best performance), the addition of 8% nanosilica and 2% polyolefin fibers to the geopolymer concrete design has improved the water permeability results by 43.99% and 55.41%, respectively. In this way First, the nanoparticles fill the pores of the matrices, which reduces the porosity of the geopolymer nanocomposites, resulting in uniformity, less pores, and a more compact geopolymer matrix [13]. Also Preventing the connection of pores and bonding the flow channels in the concrete, the polyolefin fibers strengthen it and avoid its spalling [24].

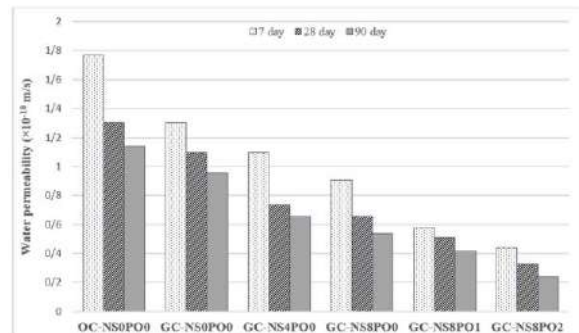


Fig. 6. The water permeability of the specimens



Fig. 7. The amount of water absorption in the specimens

3.4 Results of the SEM test

In this study, scanning electron microscope images at a scale of 500 nm were taken on concrete samples and shown in Figure 8. The volume of hydrated gels in the sample of ordinary concrete is less than that of geopolymer concrete. Cracks, cavities and unreacted particles are observed in all designs, but their amount in ordinary concrete is more than geopolymer concrete. In samples of geopolymer concrete containing nanosilica, the concrete microstructure has a better density and the volume of cavities and unreacted particles is reduced. Because First, the nanoparticles fill the pores of the matrices, which reduces the porosity of the geopolymer nanocomposites, resulting in uniformity, less pores, and a more compact geopolymer matrix [13]. In fact, the pozzolanic reaction condenses and homogenizes the microstructures by converting C-H to C-S-H [5], thus creating more geopolymer gel and a denser matrix [33]. However, further increase in NS content causes insufficient dispersion and accumulation of nano-silica particles, which slightly reduces matrix density [6]. The nano-silica addition to the geopolymer concrete increases the geopolymerization reaction. In this case, more amorphous geopolymer gel is created in the matrices. This issue, in turn, indicates that the nano-silica particles prevent the

resistance decline of geopolymer concrete[13]. The presence of some microcracks in the structure of geopolymer concrete is due to heat treatment below 60°C. But In the sample containing nano-silica, very few fine cracks are observed, in which nano-silica acts as a filler to fill the spaces inside the hardened microstructure skeleton of the geopolymer paste and increase its compaction [20,21].

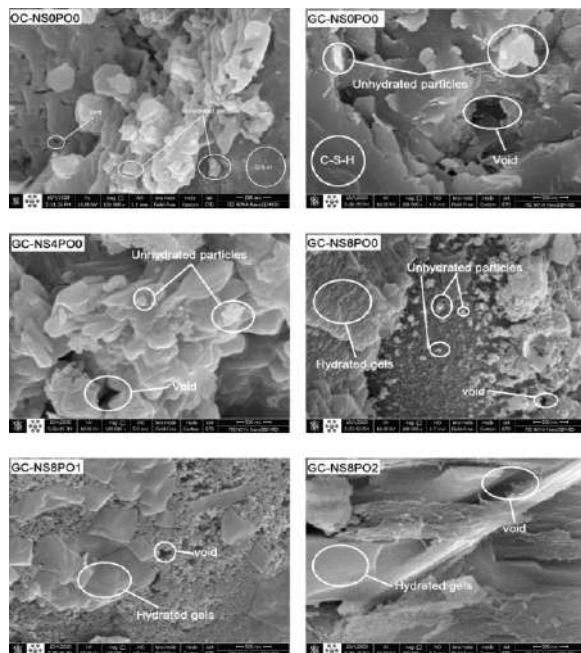


Fig. 8. Microstructure (SEM) image under room temperature

4. Conclusions

In this experimental study, compressive strength, impact strength and permeability of slag geopolymer concrete at 7 and 28 days of processing age were investigated. SEM test was performed on concrete samples at 90 days of processing age. The results of this research are as follows.

1. Increasing the curing age improved the results. In this regard, at 28 days of processing age, the lowest (55.78 M.Pa) and maximum (78.91 M.Pa) compressive strength belonged to design 1 (ordinary concrete) and design 4 (geopolymer concrete containing 8% nanosilica). At impact strength, the lowest (244.24 j) and highest (2829.15 j) impact energy obtained from Scheme 1 and Scheme 6 (geopolymer concrete containing 8% nanosilica and 2% fibers) were obtained. In the water permeability

test in concrete, the best (16 mm) and weakest (32 mm) performance belonged to Figure 6 and Figure 1.

2. At 28 days of curing age, adding up to 8% nanosilica to the geopolymer concrete composition improved the compressive strength test results by 19.01%, water permeability by up to 40.29% and impact strength by up to 36.36%.

3. Addition of up to 2% of polyolefin fibers in the composition of geopolymer concrete at the age of 28 days of curing resulted in a 28.95% decrease in compressive strength but a 20% improvement in water permeability and 50.16% in impact strength.

4. The results of all tests showed the superiority of mechanical properties and durability in geopolymer concrete compared to ordinary concrete.

5. SEM images, due to the microstructural superiority of geopolymer concrete over control concrete, covered the results of other tests in this study.

CRediT authorship contribution statement

Mohammadhossein Mansourghanaei:

Conceptualization, Methodology, Validation, Formal analysis, Investigation, Resources, Data curation, Writing - original draft, Writing - review & editing, Visualization, Supervision.

Morteza Biklaryan:

Conceptualization, Formal analysis, Resources, Data curation, Writing - original draft, Writing - review & editing, Visualization, Supervision.

Declaration of Competing Interest

The authors declare that they have no known competing financial interests or personal relationships that could have appeared to influence the work reported in this paper.

Acknowledgments

This research was done with the support of Islamic Azad University, Chalous Branch.

References

1. Nosrati, A., Zandi, Y., Shariati, M., Khademi, K., Aliabad, M., Marto, A., & Khorami, M. (2018). Portland cement structure and its major oxides and fineness. *Smart structures and systems*, 22(2), 425-432.
2. Davidovits J. Soft mineralogy and geopolymers. *Proc. 1st Int. Conf. on geopolymers*. 1988. p. 19-21. [13] Davidovits J. Geopolymers: man made rocks, geosynthesis and the resulting development of very early high strength cements. *J Mater Educ*

- 1994;16:91–139.[14] Wang H, Li Haihong, Yan F. Synthesis and mechanical properties of metakaolinite – based geopolymer. *Colloids Surf A* 2005;268:1–6.
3. Neupane, N., Chalmers, D., & Kidd, P. (2018). High-strength geopolymer concrete properties. advantages and challenges. *Advances in Materials*, 7(2), 15-25.
 4. Allahverdi, A. L. I., Ebrahim Najafi Kani, and Mahshad Yazdanipour. "Effects of blast-furnace slag on natural pozzolan-based geopolymer cement." *Ceramics-Silikáty* 55.1 (2011): 68-78.
 5. Du, H., S. Du, and X. Liu, Durability performances of concrete with nano-silica. *Construction and building materials*, 2014. 73: p. 705-712.
 6. Supit, S.W.M. and F.U.A. Shaikh, Durability properties of high volume fly ash concrete containing nano-silica. *Materials and structures*, 2015. 48(8): p. 2431-2445.
 7. Ryu, G.S., et al., The mechanical properties of fly ash-based geopolymer concrete with alkaline activators. *Construction and Building Materials*, 2013. 47: p. 409-418.
 8. Mehdipour, S., et al., Mechanical properties, durability and environmental evaluation of rubberized concrete incorporating steel fiber and metakaolin at elevated temperatures. *Journal of Cleaner Production*, 2020. 254: p. 120126.
 9. McNulty, E., Geopolymers: an environmental alternative to carbon dioxide producing ordinary Portland cement. Department of Chemistry, The Catholic University of America, 2009.
 10. Siddique, R. and D. Kaur, Properties of concrete containing ground granulated blast furnace slag (GGBFS) at elevated temperatures. *Journal of Advanced Research*, 2012. 3(1): p. 45-51.
 11. Yüksel, İ., R. Siddique, and Ö. Özkan, Influence of high temperature on the properties of concretes made with industrial by-products as fine aggregate replacement. *Construction and building materials*, 2011. 25(2): p. 967-972.
 12. Davidovits J.: US Patent No. 4509985, 1985.
 13. Assaedi, H., et al., Influence of nano silica particles on durability of flax fabric reinforced geopolymer composites. *Materials*, 2019. 12(9): p. 1459.
 14. Beigi, M.H., et al., An experimental survey on combined effects of fibers and nanosilica on the mechanical, rheological, and durability properties of self-compacting concrete. *Materials & Design*, 2013. 50: p. 1019-1029.
 15. Deb, P.S., P.K. Sarker, and S. Barbhuiya, Sorptivity and acid resistance of ambient-cured geopolymer mortars containing nano-silica. *Cement and Concrete Composites*, 2016. 72: p. 235-245.
 16. Law, D.W., et al., Long term durability properties of class F fly ash geopolymer concrete. *Materials and Structures*, 2015. 48(3): p. 721-731.
 17. Bahadori, H. and P. Hosseini, Reduction of cement consumption by the aid of silica nano-particles (investigation on concrete properties). *Journal of Civil Engineering and Management*, 2012. 18(3): p. 416-425.
 18. Bosiljkov, V.B., SCC mixes with poorly graded aggregate and high volume of limestone filler. *Cement and Concrete Research*, 2003. 33(9): p. 1279-1286.
 19. Adak, D., M. Sarkar, and S. Mandal, Structural performance of nano-silica modified fly-ash based geopolymer concrete. *Construction and Building Materials*, 2017. 135: p. 430-439.
 20. Deb, P.S., P.K. Sarker, and S. Barbhuiya, Effects of nano-silica on the strength development of geopolymer cured at room temperature. *Construction and building materials*, 2015. 101: p. 675-683.
 21. Shih, J.-Y., T.-P. Chang, and T.-C. Hsiao, Effect of nanosilica on characterization of Portland cement composite. *Materials Science and Engineering: A*, 2006. 424(1-2): p. 266-274.
 22. Gülşan, M.E., et al., Development of fly ash/slag based self-compacting geopolymer concrete using nano-silica and steel fiber. *Construction and Building Materials*, 2019. 211: p. 271-283.
 23. Their, J.M. and M. Özakça, Developing geopolymer concrete by using cold-bonded fly ash aggregate, nano-silica, and steel fiber. *Construction and Building Materials*, 2018. 180: p. 12-22.
 24. Yousefvand, M., Y. Sharifi, and S. Yousefvand, An Analysis of the Shear Strength and Rupture Modulus of Polyolefin-Fiber Reinforced Concrete at Different Temperatures. *Journal of civil Engineering and Materials Application*, 2019. 3(4): p. 238-254.
 25. Alberti, M.G., A. Enfedaque, and J.C. Gálvez, Improving the reinforcement of polyolefin fiber reinforced concrete for infrastructure applications. *Fibers*, 2015. 3(4): p. 504-522.
 26. Rashad, A.M., The effect of polypropylene, polyvinyl-alcohol, carbon and glass fibres on geopolymers properties. *Materials Science and Technology*, 2019. 35(2): p. 127-146.
 27. Rashad, A.M., The effect of polypropylene, polyvinyl-alcohol, carbon and glass fibres on geopolymers properties. *Materials Science and Technology*, 2019. 35(2): p. 127-146.

28. Wang, K., S.P. Shah, and P. Phuaksuk, Plastic shrinkage cracking in concrete materials-Influence of fly ash and fibers. *ACI Materials Journal*, 2002. 99(5): p. 512-513.
29. Olivito, R. and F. Zuccarello, An experimental study on the tensile strength of steel fiber reinforced concrete. *Composites Part B: Engineering*, 2010. 41(3): p. 246-255.
30. Islam, A., et al., Influence of steel fibers on the mechanical properties and impact resistance of lightweight geopolymer concrete. *Construction and Building Materials*, 2017. 152: p. 964-977.
31. Pilehvar, S., et al., *Physical and mechanical properties of fly ash and slag geopolymer concrete containing different types of micro-encapsulated phase change materials*. *Construction and Building Materials*, 2018. **173**: p. 28-39.
32. Ahmad, S.I. and M.A. Hossain, *Water permeability characteristics of normal strength concrete made from crushed clay bricks as coarse aggregate*. *Advances in Materials Science and Engineering*, 2017. **2017**.
33. Phoo-ngernkham, T., et al., The effect of adding nano-SiO₂ and nano-Al₂O₃ on properties of high calcium fly ash geopolymer cured at ambient temperature. *Materials & Design*, 2014. 55: p. 58-65.



Seismic reliability analysis for strengthening of reinforced-concrete hospital building with base isolation Frames

Mostafa Radmehr^a, Abbas Akbarpour^b, Muhammed Maleknia^{c*}

^aLecturer, Civil Engineering, Faculty of Islamic Azad University, (Damavand Branch), Tehran, Iran.

^bAssistant Professor, Civil Engineering, Faculty of Islamic Azad University, (South Tehran Branch), Tehran, Iran.

^cPh.D Student, Structural Orientation, Faculty of Islamic Azad University, (Chalous Branch), Mazandaran, Chalous, Iran.

Article History: Received date 15 July 2022; revised date 19 September 2022; 29 September 2022

Abstract

When an earthquake occurs in a region, it causes structural damages to buildings. Retrofitting these damaged structures before earthquakes to happen reduces the potential hazards and minimizes future casualties. In this paper, the seismic assessment of Reinforced Concrete (RC) structures inadequately to withstand seismic loads due to changing demands, and their retrofitting is studied. After a brief introduction of seismic retrofit described for existing structures, methods of assessing the seismic vulnerability of existing buildings are presented. To show the effect of the selected retrofit approach on the seismic behavior of RC buildings, an existing hospital building was selected as the case study. Since the use and occupancy of the selected RC building designed as a residential building had changed, a seismic assessment was carried out using Opensees software to show whether the building needs seismic retrofit or not. After macro modeling to assess the seismic behavior of the structure, the dynamic analysis was conducted by applying 7 earthquake records on soil type B based on Iranian seismic code. Selecting the retrofit approach, which contains using Lead Rubber Bearing (LRB), was performed based on Iranian codes. To consider the uncertainties related to the ground motion, 27 ground motion time histories were utilized and results showed that the building needs seismic retrofit because of the increasing demands. Furthermore, the performed reliability study illustrated an effective role in improving the seismic behavior of the buildings under earthquake loads by the retrofit method. © 2017 Journals-Researchers. All rights reserved.

(DOI:<https://doi.org/10.52547/JCER.4.3.40>)

Keywords: Reliability analysis, Seismic Assessment, Retrofit, RC Structure, LRB, Monte Carlo Simulation

* Corresponding author. Tel.: +989113396652; e-mail: mohamad_maleknia@yahoo.com.

Introduction

In the event of an earthquake, structures move in all directions. The most severe damages inflicted upon buildings are caused by lateral movements, which cause the large displacements and disturb the stability of the structure. The importance of seismic assessment and rehabilitation of existing buildings is due to the existence of a large number of inadequate existing structures in earthquake regions. In recent years, quite a lot of research activities have been focusing on this topic and various guidelines and seismic codes have given considerable attention to such buildings [1, 2]. In some cases, the studied buildings by researchers needed strengthening to maintain their performance level for stronger earthquakes, so they are required to be retrofitted. The retrofit method should meet the requirements and criteria by considering the cost, time, and quality. Several approaches such as FRP wrapping of columns and joints, steel or RC jacketing, and shear walls have been developed in previous studies to retrofit RC structures [3, 4]. Many types of research have been undertaking studies to evaluate the performance of the seismic isolation systems which are one of the most practical passive systems in controlling the structural vibrations. Kramer [6] investigated 3-, 7-, and 12-story frames in cases without and with isolator (LRB) using the IDA analysis. Then, the effect of (LRB) isolator was separately determined in the reinforced concrete structures using a fragility curve under 7 earthquakes near and far-fault. Shakib and Fuladgar [7] examined the effect of triple components of earthquake acceleration on the response of the isolated structure in the base by sliding frictional seismic isolator undergoing three components of El-Centro 1940, Tabas 1978, and Northridge 1994 earthquakes. In the last two decades, quite a lot of researches has concentrated on the field of structural reliability theory. Afshan et al. [8] carried out a reliability analysis on structural stainless steel according to EN 1990 Annex D, they collected a valuable data based on statistical material and structural performance on stainless steel structural elements, finally, they suggested these data for using in reliability analysis

of stainless steels. Zhang et al. [9] presented a system-based, analysis method which is introduced as "Direct Design Method" (DDM), in this method a reliability framework has been developed which is a simple First-Order Reliability method versus the costly Monte Carlo method is verified. Hao et al. [10] in this study, is proposed an algorithm of non-probabilistic reliability-based design optimization (NRBDO), The algorithm illustrates that this proposed method applies to structures that are engineering complex as well as the uncertainty distribution of information is not available. Fu et al. [11] used a novel approach to optimize wind resistance in high-rise buildings considering the uncertainties in wind speed, natural frequency of structures, damping and the joint distribution of the wind speed and direction as well as using a new model of earthquake acceleration. The results of this research show that this method could reduce the total weight of the high-rise buildings. Pirizadeh and Shakib [12] provided a framework for improving the performance of special steel moment-resisting frame (SMRF) setback structures based on the reliability method, for this purpose using the results of incremental dynamic analysis (IDA), an algorithm that follows a highly accurate equation, which enables to calculate the maximum inelastic inter-story drift ratio of setback structures. They demonstrated that this economical technique can reduce the potential damage to SMRF frames, which is located in an effective seismic area. Gaxiola-Camacho et al. [13] presented a novel approach for Performance-Based Seismic Design (PBSD) procedure as well as reliability analysis. They applied 20 records on a 9-story steel frame and using 300 deterministic analysis and 600,000 cycles of Monte Carlo simulations (MSC). Their findings, which are criteria the probability of failure for limit states, proved the accuracy of their proposed algorithm. Castaldo et al. [14] evaluated a concrete structure, which has been equipped by with single-concave friction pendulum, they considered the elastic response pseudo-acceleration corresponding to the isolated period as a one of the variable random and also using Latin Hypercube Sampling for calculation of seismic reliability as well as the seismic robustness. Their results provided appropriate design recommendations for a concrete structure system equipped with FPS.

Risi et al. [15] proposed a novel multi-dimensional limit state function damage criteria for evaluating the seismic performance of reinforced concrete structures. They showed that in a linear state, there is not highly change in fragility and risk curves, while in the nonlinear state for the probability of failure, the range of variation is between 10 to 50 percent. Homami and Aghakouchak [16] studied a novel approach to mixing reliability and fuzzy method to consider the reliability of a rigid steel frame according to the Iranian steel frame codes. They calculated the reliability index as well as presented standard recommendations for using this kind of moment-resisting steel frame, which is widely used in Iranian buildings. Furthermore, many studies have been carried out to assess the reliability of structures with different methods such as fuzzy reliability analysis [17-27], which in this method, the application of fuzzy set theory in structural engineering is investigated. This paper illustrates a study regarding an existing RC building which is a hospital located in Iran. The performance of the structure was evaluated employing linear static and dynamic analyses using OPENSEES 2.6. Structural modeling was based on the Monte Carlo Simulation (MCS) by defining the shear wall as shell elements. Static and dynamic analyses (spectral analysis) have been carried out based on Iranian seismic code (Standard 2800) [5]. Uncertainty is considered in the important structural parameters, including the compressive strength of concrete, the tensile strength of reinforcing bars, and effective stiffness in LRB. For seismic analysis, 27 different models were considered based on the values of uncertain structural parameters from the Monte Carlo Simulation method. These models were analyzed under various earthquake records using OPENSEES. After the seismic evaluation, it was revealed that the building needs to be retrofitted. Since applicability, cost and, time are very important in the rehabilitation methods, two approaches namely steel jacketing and RC shear wall were selected to be used for this structure. Additionally, it was found that both solutions solved the problem partially; because in solution one, some columns were still not strong enough and in solution two the inter-story drift was not allowable. Thus, the final solution is using LRB to reduce the seismic demand of the structure. Besides, to show the effect

of structural parameters, a reliability study was undertaken.

2. Structural Modeling

The modeling and analysis of the buildings were conducted via OPENSEES version 2.6, which implements the finite element method for solving partial differential equations [28]. The software has the capability of macro modeling of building structures with high speed in the nonlinear dynamic analysis. OPENSEES 2.6—the nonlinear analysis program—was used to model the CM building to calculate the vulnerability. At first, the existing building was modeled by SAP2000. Then, to show the damage to the building in the nonlinear dynamic analysis under the earthquake records, it was modeled in OPENSEES 2.6. Structural information in this research as a case study model has been considered as the total area of the building is 9600 square meters and also the rectangular shapes were used for the beams (40x40, 40x45 and 40x50 square centimeters) and columns (40x40, 40x45, 40x50, 40x55, 40x60, 40x65, 40x70 and 40x80 square centimeters), and reinforcement bars for beams was $\phi 20$ and for columns were $\phi 20$ and $\phi 22$, with different reinforcement bar numbers. Furthermore; the shear walls were modeled with shell elements to consider out-of-plane stiffness. Fig.1 shown the configuration of column and shear walls in this research. Since the building has already been constructed, it is necessary to examine the material properties, especially the concrete compressive strength; and that is due to the low quality of cast-in-situ RC buildings. Therefore, one concrete core test and two Schmidt hammer tests in each story have been performed randomly. The results show that the lowest, highest and average value of concrete compressive strength are 14, 21, and 18 N/mm² respectively, hence the average value—18N/mm²—was used in the structural modeling and assessment. The yield stress for longitudinal reinforcements and stirrups (f_y) were assumed 400 and 300 N/mm², respectively also the unit weight of concrete and the Poisson's ratio for concrete considered 24 kN/m³ and 0.15 respectively. To protect the reinforcement against corrosion and

fire concrete cover to reinforcement bars based on Iranian concrete code it was applied 50 mm.

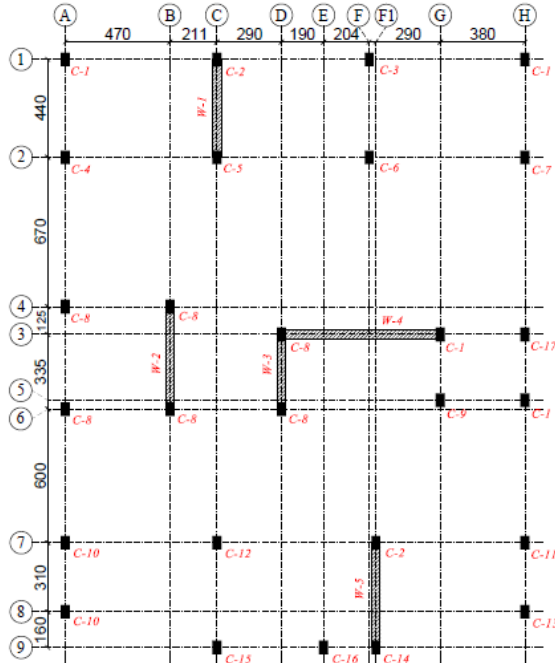


Fig. 1. The plan of the existing building and labeling of columns and shear walls

3. Sampling Methods

Various techniques are available to calculate the key parameters in the structural reliability method, in which sampling methods are one of the most important ones. The main advantage of the sampling methods is evident when the closed-form of the limit-state function is not available for the structure. Enhancing the safety and limiting the uncertainties in the design of structural systems is a matter of importance. The structural reliability is employed as a probabilistic criterion to evaluate the reliability of structural systems. To describe the system behavior and identify the relationship between the basic parameters in a structural system, the limit state function of the system has to be determined. Using the time-invariant reliability analysis procedure, the probability of failure can be determined by Eq. 3.1. In which, $g(X)$ is the limit state function, Pf the

probability of structural failure, and $f_x(X)$ is defined as the probability density function.

$$Pf = P[g(X) \leq 0] = \int \dots \int_{g(X) \leq 0} f_x(X) dX \quad (3.1)$$

This equation can be rewritten as below:

$$Pf = \int \dots \int I[X] f_x(X) dX \quad (3.2)$$

Where, $I[X]$ is an indicator function $I(x_i)$ is defined in Eq. 3.3, which is regarded as an indicator for considering successful or unsuccessful simulations.

$$I[X] = \begin{cases} 1 & \text{if } g(X) < 0 \\ 0 & \text{if } g(X) \geq 0 \end{cases} \quad (3.3)$$

Evaluating analytically for complex or large-scale structures is practically impossible since there are no closed-form expressions, the best technique is the numerical solution method by the Monte Carlo Simulation (MCS). Although MCS has a high computational cost, it is regarded as an effective method and is widely utilized for the evaluation of the probability of failure in computational mechanics, either to compare with other methods or as a self-contained reliability analysis tool. When the analytical solution is not feasible and the limit state function cannot be expressed or estimated analytically, the MCS technique is used. This method is mostly the case in complex problems with a large number of basic variables where other reliability analysis methods are not suitable. If we express the limit state function as $g(x) < 0$, which is the vector of the random variables. The joint probability of failure for all random variables is defined by Eq. 3.4, which gives an unbiased estimator of the probability of failure.

$$Pf = \frac{1}{n} \sum_{i=1}^n I[x_i] \quad (3.4)$$

In structural reliability, while using simulation methods, evaluating the probability of failure is important for a specified performance function efficiently and accurately. With the help of limit state

function $G = C - D$, which in this study defined by subtraction of the maximum inter-story drift as the demand (D) from the allowable inter-story drift (C) which is limited to the life safety limit according to FEMA 356 as the capacity, it is easy to determine the probability of failure from relation 3.5. In this respect, is the number of times that the function G is negative (failure) to N which is the total number of iterations of analysis.

$$Pf \cong \frac{N_s}{N} \quad (3.5)$$

Finally, Reliability Index is determined by Eq. 3.6.

$$\beta = \Phi^{-1}(Pf) \quad (3.6)$$

Although the mathematical formulation of MCS is relatively simple and can handle practically every possible case, regardless of its complexity, the computational effort involved in conventional MCS is excessive. For this reason, a lot of sampling techniques, also called variance reduction techniques, have been developed to improve the computational efficiency of the method by minimizing the sample size and reducing the statistical error that is inherent in MCS. Among them is the importance of sampling Latin Hypercube Sampling provides a limited sampling plan instead of random sampling in the direct simulation. In this method, the interval from 0 to 1 is divided into N equal parts and one sampling point is generated from each part, which the probability of events is the same in each part. To generate input random variables inverse transformation is used which have been shown by Eq. 3.7.

$$u_i = \frac{u}{N} + \frac{i-1}{N} \quad (3.7)$$

In which, u is a random parameter in the interval (0, 1) and $u_i (i = 1, 2, \dots, N)$ is the random value for the i -th interval. Then, a value of each input variable is selected accidentally and put into the limit state function. This procedure is repeated for N times to calculate of probability of failure.

4. Static Analysis

The model was analyzed for dead, live, and seismic loads using Opensees. The assessment and retrofit designs have been carried out according to the requirements of Iranian codes. As the building was used to be residential, now that it is used as a hospital building the live and dead loads would be greater. Dead load is 550 kg/m² and live loads are 300, 350, 400 and 500 kg/m² based on Iranian codes. The seismic load is defined as shown in Fig. 2 according to the equivalent static load. Because the building use has been changed from residential to the hospital and the period of the structure has been changed due to strengthening, hence two main differences in the building before and after retrofitting are: Importance factor (I) and Spectral parameter (B). To consider dynamic analysis, the spectrum should be defined based on Standard 2800 and soil type II ($375 < V_s < 750$). The spectrum is shown in Fig. 2.

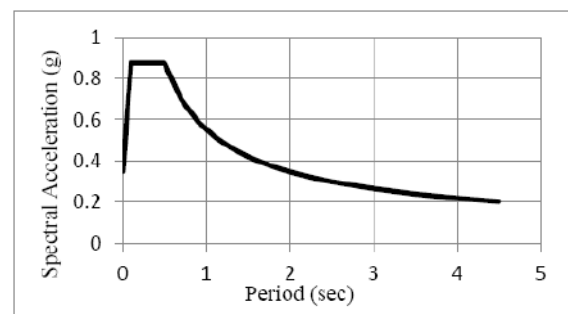


Fig. 2. The spectrum curve for dynamic analysis

Based on Standard 2800, the maximum inter-story drift should be less than 0.45%. However, Story 4-15 had higher drift than the allowable value in X and Y directions. Table 1 shows the drift ratio in X and Y directions. To check the torsion of the building, eccentricity in X and Y directions should be less than 20% of the width and length of the building in the plan. By considering 21.07m wide and 26.7m long, the allowable eccentricities are 4.2 m and 5.34 m in X and Y directions respectively. The results show that the eccentricity in the X direction is exceeding the allowable value. There is no problem regarding the overturning and stability of the structure. Besides, the

allowable DCR is one, whereas in many columns and shear walls DCR is higher than one. It should be noted that vertical seismic loads, the simultaneous effect of seismic loads in both directions, and allowable beams deflections, have not been considered in the existing structure design.

5. Dynamic Analysis

Since DCR in some elements is greater than the allowable value prescribed by the seismic code, the dynamic analysis must be carried out to evaluate the structure and see if it requires retrofitting. In this paper, time history analysis is employed to perform the nonlinear dynamic analysis based on 7 earthquake records on soil type B, which is the soil type on which the building is built. Table 1 shows the selected records which are taken from FEMA-P695 [29]. Having been selected based on the soil type and frequency content, records were scaled to a standard design spectrum using Iranian seismic code (Fig. 3).

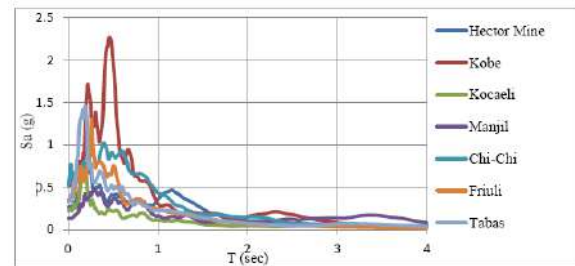


Fig. 3. Earthquake spectra on soil type B

Maximum inter-story drift, as one of the most important structural parameters indicating the performance of structures, was chosen to represent the seismic performance of the building. After applying 7 earthquake records, therefore, the maximum inter-story drift of the structure was calculated and compared before and after the retrofit. To show the performance level of the structure, 3 levels were considered based on FEMA 356 [29]. According to this standard, attributed drift to the level of Immediate Occupancy (IO), Life Safety (LS), and Collapse Prevention (CP) were 1%, 2% and 4% for RC frames respectively. The allowable seismic performance level of hospitals is IO and all of the non-structural elements should not have a performance level higher than this level. In other words, the maximum inter-story drift of this building must be lower than 1%. Fig. 4 and Fig. 5 shows the response of the structure before retrofitting in each direction.

Table 1. Selected earthquake records on soil type B

Name, Station	Vs (m/s)	USGS soil type	Fault	R (km)	M	PGA (g)
Hector Mine, Hector SCSN	685.0 0	B	Strike-slip	26.50	7.10	0.27
Kobe, Japan Nishi-Akashi CUE	609.0 0	B	Strike-slip	8.70	6.90	0.51
Kocaeli, Turkey Arcelik KOERI	523.0 0	B	Strike-slip	53.70	7.50	0.22
Manjil, Iran Abbar BHRC	724.0 0	B	Strike-slip	40.40	7.40	0.13
Chi-Chi, Taiwan TCU045 CWB	705.0 0	B	Thrust	77.50	7.60	0.51
Friuli, Italy Tolmezzo	425.0 0	B	Thrust	20.20	6.50	0.35
Tabas, Dayhook	659.0 0	B	Thrust	13.90	7.35	0.33

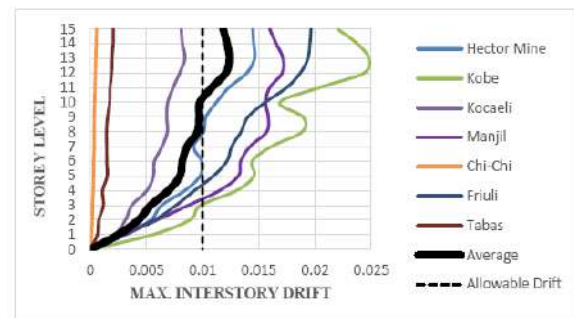


Fig. 4. Maximum inter story drift before retrofit in X direction

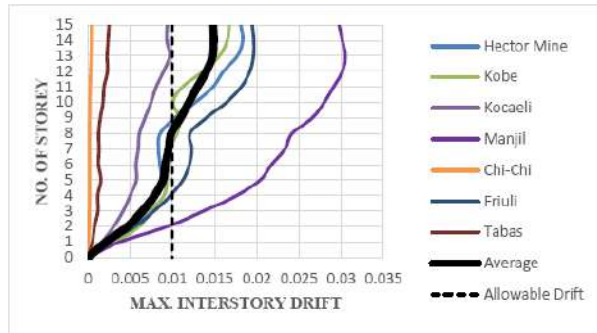


Fig. 5. Maximum inter story drift before retrofit in Y direction

The maximum inter-story drift diagrams show that the performance level of the structure is not IO which is not allowable for hospitals. Performance level in the lower stories story one to 8 is acceptable (IO). However, in the upper stories, it is not acceptable because the performance level is LS. Fig. 4 shows that Kobe earthquake causes the most damages to the structure in the X direction, whereas Manjil is the most vulnerable ones in the Y direction.

6. Retrofit Plan

To retrofit RC structures, there are several methods such as FRP wrapping of columns and joints, steel or RC jacketing, shear walls, and so forth. In each retrofit procedure, one of them has to be selected by considering all factors such as efficiency, cost, time of execution, and so on. Among all the methods, two approaches, steel jacketing and shear wall, were selected due to their low cost as well as execution time and high efficiency in RC building, especially in Iran. To show the retrofit plan of this structure, some steps are considered to yield the best results, at first, decreasing the total horizontal seismic load, secondly, reducing drifts and eccentricity of building as well as reducing DCR of all elements, in the following improving all defects in execution and finally rehabilitation of the foundation have been considered. In the first step, the best solution to decrease the total horizontal seismic load is adding shear walls on top of the foundation to increase the base shear and decrease the seismic load. These shear walls also can be known as retaining walls to

withstand soil pressure. By adding retaining walls in the 1st and 2nd stories, unallowable drifts and eccentricity of the building were solved. In addition, since these shear walls carried the shear loads in these levels, DCR of all the elements decreased.

For the rest of the stories, there were two main problems—unallowable drifts and high DCR in columns. Each selected retrofit approach, shear walls and steel jacketing, does not solve all the problems solely. In other words, although steel jacketing can reduce DCR in columns, it cannot reduce drift perfectly. On the other hand, shear walls can reduce drift while some columns fail under seismic loads. Thus, the best result is a combination of two selected retrofit approaches.

First of all, some shear walls were added in all stories to reduce drift, eccentricity, and DCR in columns in which architectural limitations such as creating openings in shear walls as facades were also considered. After designing the added shear walls and reducing the drift and eccentricity solely to the allowable values, some columns still had high DCRs. Steel jacketing solves this problem by confining concrete, making a composite section. Fig. 6 and Fig.7 show the plan of the building retrofitted by shear walls and steel jacketing.

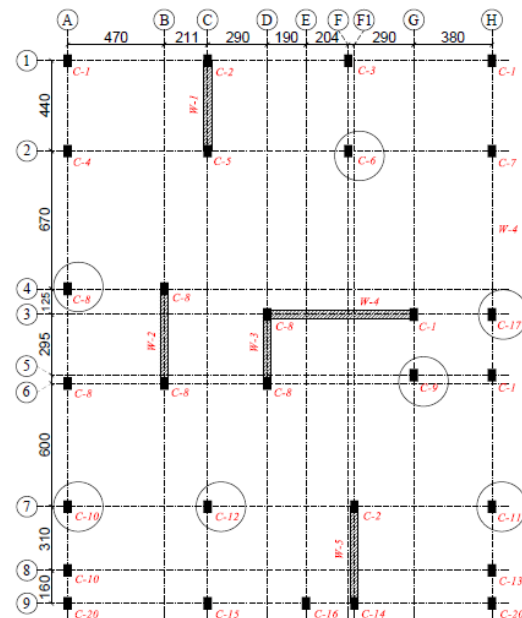


Fig. 6. Plan of the building retrofitted by shear walls and steel jacketing



Fig. 7. The building retrofitted by steel jacking

As shown in Fig. 6, column C20 was added to the structure to complete the surrounding shear walls in stories 1 and 2. One of the main issues in adding shear walls to an existing RC building is the connection to the foundation. The next step in the retrofit plan is remedying all the defects caused by the faulty execution of the building and construction work. As mentioned before, the test results of the compressive strength of concrete show that the average value is 18 MPa, which was used in the modeling. After retrofitting the structure, the final step is the rehabilitation of the foundation because adding and increasing new loads may cause higher demands in the foundation. To solve these problems, it should be mentioned that using LRB can be useful in reducing demands instead of increasing the capacity of strengthening of structural elements.

7. Base Isolation

The use of isolators with a performance similar to that of horizontal springs decreases the earthquake forces and resonates with dominant frequency content

by changing the inherent period of structures. The concept of increasing the period of a structure is the same as using isolators [30]. Seismic isolation is one of the many different ways to resist the earthquake load, which increases the time period of structure and force transfer interruption path [31]. The lead-rubber isolator has been more prevalent among isolator systems and has been widely used in many countries. These isolators contain some layers of steel and rubber plates with the lead bar which is embedded in a few holes. The lead cores deform at shearing stress with a magnitude of 10 MPa, expressing a hysteresis behavior with a two lines response generated in the lead (Fig. 8). The role of this lead core is energy dissipation, which ultimately decreases the amount of isolator displacement; thus, it can be called an auxiliary damper [32] (Fig. 8).

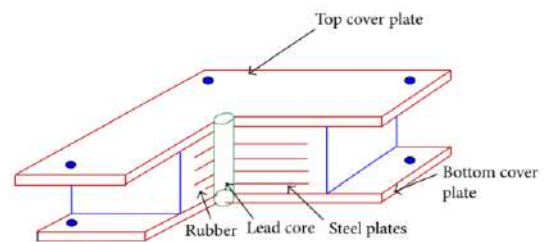


Fig. 8. Schematic of Rubber isolators with lead core [32].

In this study, the used isolator system is the rubber isolator with lead core. To design the isolators, the effective damping, design time period, effective horizontal stiffness, and the maximum horizontal displacement of support have been calculated based on design shear strain. Isolators have been designed based on FEMA356 for these weak hospital buildings. The LRB hysteretic model was assumed to be bilinear with first stiffness k_1 and secondary stiffness k_2 as illustrated in Fig. 9. The ratio of the primary stiffness to the secondary stiffness (k_1/k_2) is assumed to be 10 [33, 34]. The characteristics of designed LRB isolators are listed in the next section based on Monte Carlo simulation.

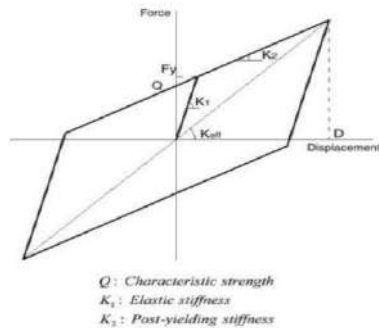


Fig. 9. LRB hysteresis behavior

The analytical spring models (zero length element) which is usually employed for simulating the behavior of LRB devices, were constructed with the OpenSees (Fig. 10). In this study, “KikuchiAikenLRB” material which produces nonlinear hysteretic curves of lead-rubber bearings has been assigned to the spring.

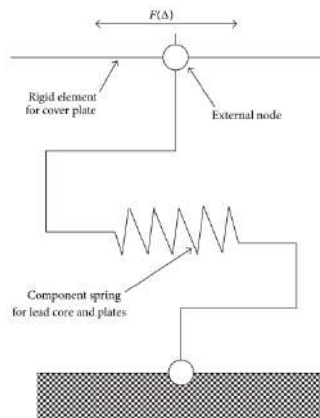


Fig. 10. Analytical model for component spring (LRB model) [35].

8. Results And Descussion

To consider uncertainty in structural parameters, first, a probabilistic distribution was assigned to each of them [36]. Then, by using the Monte Carlo Simulation method [36], 3 different values have been generated for each structural parameter. These parameters, with their assigned average value, type of

distribution function, and coefficient of variation, are shown in Table 2. The value of average compressive strength of concrete was assumed based on Iranian seismic code (Standard 2800) and Iranian concrete code [5]. The base isolation design parameters have presented in Table 3.

Table 2. Random variables

Parameters	Average Value	Standard Dev.	Distribution Function Type
Compressive Strength of Concrete	25 MPa	3	Normal
Tensile Strength of Reinforcing Bars	400 MPa	20	Log-Normal
Effective Stiffness of LRB	3000 kN/m	1000	Normal

Table 3. Design of base isolation

ξ	Td (sec)	Q/W	K eff (kN/m m)	DD (m)	Ap (cm ²)	A0 (cm ²)
0.1	2.5	0.03	5679.1296	0.30535	331.0875	11803.48
0.26	2.5	0.06	5679.1296	0.229013	662.175	11803.48
0.48	2.5	0.09	5679.1296	0.185061	993.2625	11803.48
0.19	4	0.03	2218.41	0.398824	331.0875	11803.48
0.52	4	0.06	2218.41	0.293136	662.175	11803.48
0.78	4	0.09	2218.41	0.293136	993.2625	11803.48
0.3	5.5	0.03	1173.373884	0.474191	331.0875	11803.48
0.71	5.5	0.06	1173.373884	0.403062	662.175	11803.48
1	5.5	0.09	1173.373884	0.403062	993.2625	11803.48

After seismic evaluation and determining the unallowable values of structural parameters such as DCR and Drift ratio, seismic rehabilitation was used to reduce the demands and meet the criteria of the regulations. By using LRB, the result of this procedure can be shown as follows based on the mentioned steps:

1. As mentioned before the low compressive strength of concrete was considered in modeling.

2. 27 models were evaluated with 3 different structural parameters based on Monte Carlo method.

3. By using steel jacking in retrofitting columns, all DCRs were reduced below 1. Some columns had allowable stresses due to adding shear walls and the 12 remaining columns were strengthened by using steel jacking.

4. Due to the soil loads, a retaining wall surrounded the building so that the base level was changed to be at the second story.

5. Retrofit approach causes the seismic performance of the structure to be IO level in the hospital based on FEMA-356. Fig. 11 and Fig. 12 show the response of structure after retrofitting in each direction.

After seismic assessing, designing, and retrofitting of the hospital building, the instructions were given to the retrofit constructor to execute all of them.

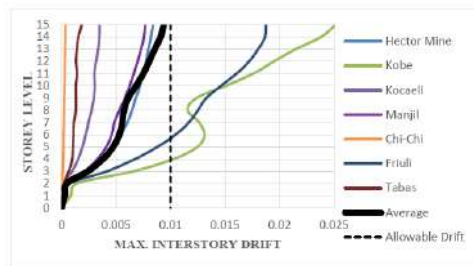


Fig. 11. Maximum inter story drift after retrofit in X direction

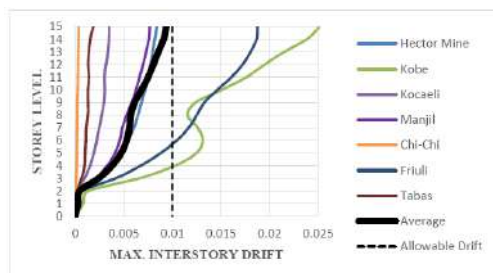


Fig. 12. Maximum inter story drift after retrofit in Y direction

As illustrated in figures above, time history analysis after retrofit shows that average drift of structure is less than 1% in both directions. Because of changing the first mode behavior of the structure and its period, only in two earthquake records (Friuli and Kobe) the maximum drift is higher than

allowable value. Moreover, the drift of story 1 and 2 is about zero, which is because of the retaining wall that reduces the drift considerably in these two stories. The maximum inter-story drift diagrams show that the performance level of the structure is not IO which is not allowable for hospitals. Performance level in the lower stories story one to 8 is acceptable (IO). Finally, to show the effect of random analysis of structural parameters and in order to calculate the reliability index of systems, two different steps can be presented, the performance failure functions as ($G = \text{Capacity} - \text{Demand}$) which demand was considered as the maximum inter-story drift and Capacity was regarded as the allowable inter-story drift according to Iranian seismic code (Standard 2800), also in order to consider capacity and demand, Monte-Carlo sampling technique was employed. However, it must be considered that extracting this close form failure function will not be easy and most of the time is available only for linear elastic system. Also by using dynamic nonlinear analysis, the seismic demands and structural resistance are evaluated under earthquake excitation. It would be practical to conduct nonlinear time-history and then calculate desired performance level or failure. By considering average values of all 27 random models under 7 earthquake and drawing the probability density function (PDF) for the performance failure functions (G) shown in Fig. 13 and Fig. 14 the reliability factor has been calculated by Eq. 3.6 which are 1.48 before retrofitting and 1.96 after retrofitting in X direction, and 1.28 and 1.59 in Y direction, which also presented in Table 4 and Table 5.

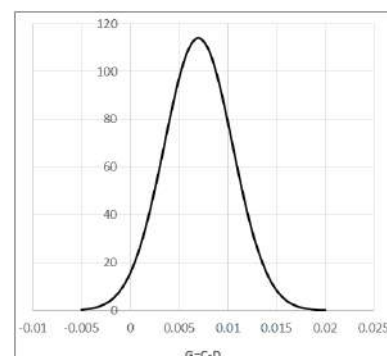


Fig. 13- Performance failure functions (G) in X direction

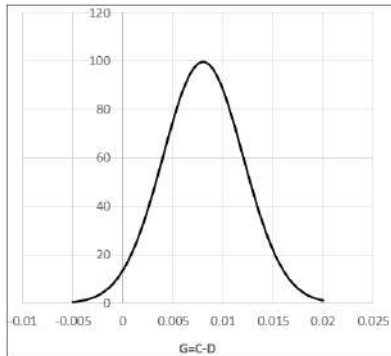


Fig. 14- Performance failure functions (G) in Y direction

Table 4. Performance failure functions (G) in X direction

Statistical characteristic	G (Limit-state function)=C-D
distribution function	Normal
Mean	0.0068
Standard deviation	0.00346
Reliability index in X direction	1.96

Table 5. Performance failure functions (G) in Y direction

Statistical characteristic	G (Limit-state function)=C-D
distribution function	Normal
Mean	0.0075
Standard deviation	0.0047
Reliability index Y direction	1.59

9. Conclusion

A seismic evaluation was performed to assess the vulnerability of a 15-story hospital building, which had been a typical residential apartment and changed to be used as a hospital. This assessment was

undertaken using Opensees software based on macro modeling. The low compressive strength of concrete in tests Schmidt hammer, and Core test, and static as well as dynamic analyses show that the building must be retrofitted. Because applicability, cost, and time are very important in rehabilitation methods, using LRB is selected as the retrofitting approach. In addition, by considering 5 steps as the strategy of the retrofit procedure, all problems such as high base shear, unallowable drift, eccentricity, DCR, and defects in construction have been solved. To show the seismic performance of the structure, time history analysis was carried out using 7 earthquake records on soil type B. The maximum inter-story drifts before retrofit is more than 1% and not allowable for hospitals because this drift is within LS performance level. However, after retrofit, this value is reduced to 1% so that the seismic performance level of the structure is IO. It should be mentioned that the maximum drift in the lower stories surrounded by retaining walls must be about zero so that the base level would be on story 2. Furthermore, retrofitting and strengthening of structures change structural parameters so that they might be damaging for structures. For instance, before retrofit, Manjil and Kobe earthquake records inflict the most damages on the structure. However, after retrofit, Kobe and Friuli are the most vulnerable ones.

References

- [1] Sattar S, Liel AB. Seismic performance of reinforced concrete frame structures with and without masonry infill walls. In: 9th US National and 10th Canadian conference on earthquake engineering, Toronto, Canada. 2010
- [2] Frosch RJ, Li W, Jirsa JO, Kreger ME. Retrofit of non-ductile moment-resisting frames using precast infill wall panels. *Earthquake Spectra* 12(4); 1996: 741–760
- [3] Papanicolaou CG, Triantafillou TC, Papathanasiou M, Karlos K. Textile reinforced mortar (TRM) versus FRP as strengthening material of URM walls: out-of-plane cyclic loading. *Mater Struct.* 41; 2008:143–157
- [4] El-Gawady M, Lestuzzi P, Badoux M. A review of conventional seismic retrofitting techniques for URM. In: 13th international brick and block masonry conference. 2004
- [5] Standard 2800 (2017), Iranian Seismic Code
- [6] S. L. Kramer, *Geotechnical Earthquake Engineering*, Prentice-Hall, 1996.

- [7] H. Shakib and A. Fuladgar, "Response of pure-friction sliding structures to three components of earthquake excitation," *Computers and Structures*. 81; 2003:189–196.
- [8] Afshan S, Francis P, Baddoo N.R, Gardner L. Reliability analysis of structural stainless steel design provisions. *Journal of Constructional Steel Research*. 114; 2015: 293-304.
- [9] Zhang H, Shayan S, Rasmussen K, Ellingwood B. System-based design of planar steel frames, I: Reliability framework. *Journal of Constructional Steel Research*. 123; 2016: 135-143.
- [10] Hao P, Wang Y, Liu C, Wang B, Wu H. A novel non-probabilistic reliability-based design optimization algorithm using enhanced chaos control method. *Computer Methods in Applied Mechanics and Engineering*. 318; 2017: 572-593
- [11] Fu J, Zheng Q, Huang Y, Wu J, Pi Y, Liu Q. Design optimization on high-rise buildings considering occupant comfort reliability and joint distribution of wind speed and direction. *Engineering Structures*. 156; 2018: 460-471.
- [12] Pirizadeh M, Shakib H. A framework is proposed to improve seismic performance of special steel moment resisting frame (SMRF) setback structures based on the reliability-based approach. *International Journal of Steel Structures* 19; 2019: 58–70.
- [13] Gaxiola-Camacho J, Azisoltani H, Villegas-Mercado F, Haldar A. A novel reliability technique for implementation of Performance-Based Seismic Design of structures. *Engineering Structures* 142; 2017: 137-147.
- [14] Castaldoa P, Mancinia G, Palazzob B. Seismic reliability-based robustness assessment of three-dimensional reinforced concrete systems equipped with single-concave sliding devices. *Engineering Structures* 163; 2018: 373-387.
- [15] Risi R, Goda K, Tesfamariam S. Multi-dimensional damage measure for seismic reliability analysis. *Structural Safety* 78; 2019: 1-11.
- [16] Homami P, Aghakouchak A. Seismic Reliability Analysis of Moment Resisting Steel Frames. *Journal of Seismology and Earthquake Engineering (JSEE)*. 9; 2008: 183-192.
- [17] Wu HC. Fuzzy reliability estimation using Bayesian approach. *Computers & Industrial Engineering* 46; 2004: 467-493.
- [18] L Li, Z Lu. Interval optimization based line sampling method for fuzzy and random reliability analysis. *Appl. Math. Model.* 38:2014;3124–3135.
- [19] Li G, Lu Z, Jia X. A fuzzy reliability approach for structures based on the probability perspective. *Struct Saf* 2015; 54:10–18.
- [20] Purba JH, Lu J, Zhang G. A fuzzy-based reliability approach to evaluate basic events of fault tree analysis for nuclear power plant probabilistic safety assessment. *Fuzzy Set Syst* 2014; 243:50–69.
- [21] Ni Z, Qiu Z Hybrid probabilistic fuzzy and non-probabilistic model of structural reliability. *Comput Ind Eng* 58(3); 2010: 463–467.
- [22] Canizes B, Soares J, Vale Z Hybrid fuzzy Monte Carlo technique for reliability assessment in transmission power systems. *Energy* 45; 2012:1007–1017
- [23] Biondini F, Bontempi F, Malerba P.G. Fuzzy reliability analysis of concrete structures. *Computers and Structures* 82; 2004:1033–1052.
- [24] Bing L, Meilin Z, Xu K. A practical engineering method for fuzzy reliability analysis of mechanical structures. *Reliability engineering and system safety* 67; 2000:311–315.
- [25] Jiang Q, Chen C.H. A numerical algorithm of fuzzy reliability. *Reliability engineering and system safety* 80; 2003:299–307.
- [26] Gu X, Lu Y. A fuzzy-random analysis model for seismic performance of framed structures incorporating structural and non-structural damage. *Earthquake engineering and structural dynamics* 34; 2005:1305–1321.
- [27] Onisawa T, Kacprzyk J. Reliability and safety analysis under fuzziness. Springer Co. 1955.
- [28] S. Mazzoni, F. McKenna, M. H. Scott, G. L. Fenves, et al., "OpenSees Command Language Manual", July, 2007.
- [29] Federal Emergency Management Agency (FEMA). "Prestandard and Commentary for the Seismic Rehabilitation of Buildings", Report No. FEMA 356, FEMA, Washington, D.C. (2000)
- [30] R. L. Mayes and F. Naeim, "Design of structures with seismic isolation," in *The Seismic Design Handbook*, pp. 723–755, Springer, 2001.
- [31] Y. Wang, "Fundamentals of seismic isolation," in *Proceedings of the International Training Programs for Seismic Design of Building Structures*, pp. 139–149, Taipei, Taiwan, 2003.
- [32] C. S. Tsai, "Advanced base isolation systems for light weight equipments," in *Earthquake Resistant Structures—Design, Assessment and Rehabilitation*, pp. 79–130, InTech, 2012.
- [33] Federal Emergency Management Agency (FEMA) P695, "Quantification of Building Seismic Performance Factors", June 2009.
- [34] Farzad Naeim (ed.), *The seismic desing Handbook(2nd Edition)*, 2000
- [35] J.W. Hu, "Response of seismically isolated steel frame buildings with sustainable lead-rubber bearing (LRB) isolator devices subjected to near-fault (NF) ground motions," *Sustainability (Switzerland)*, vol. 7, no. 1, pp. 111–137, 2015.
- [36] R.Y. Rubinstein, "Simulation and the Monte Carlo Method", John Wiley & Sons, New York, NY 1989.



Investigation of explosive loading and its type of operation

Sadeghian S.  ^a*

^aPhD Student, Structural Orientation, Faculty of Islamic Azad University (Chalous Branch), Mazandaran, Chalous, 4651141433, Iran.

Article History: Received date 28 July 2022; revised date 25 September 2022; 11 October 2022

Abstract

The subject of evaluating the vulnerability and strengthening of structures against various natural and artificial factors such as earthquake, wind, fire and explosion, etc., has been the focus of most civil engineering researchers in recent years. However, the engineering profession is generally not well aware of the design of static or dynamic structures to resist the explosion. In this research, it has been done by presenting materials about the introduction of explosion and the components of this type of loading, and by examining the parameters in explosive loading and the relationship between them, Review and presentation of comprehensive information in this regard has been discussed. © 2017 Journals-Researchers. All rights reserved.

(DOI:<https://doi.org/10.52547/JCER.4.3.52>)

Keywords:blast load, blast wave, scale, retrofitting, modeling

1. Introduction

The explosion can threaten human life, it can also cause damage to residential and industrial buildings and cause the loss of security, communication, transportation system, and services. Since Iran is located on the earthquake belt, seismic behavior is often considered in the design of buildings. However, the engineering profession in general is not well aware of the design of static or dynamic structures for blast resistance, because in the past the blast load was rarely considered an important factor in building design, and the dynamic effects of the blast structure were only research subjects in a limited number of laboratories. It was working. The cost of creating a safe environment for explosion research is high, and for this reason, certain organizations such as military agencies, government research facilities, and large

industrial explosives factories work in this field. More than a few decades have passed since the introduction of computational tools based on the finite element method in the analysis and design of structures, but there is still a lack of a suitable tool in this field that can accurately analyze the structure against explosive loads. Also, in the new design methods, more detailed analyses will be needed to better estimate the capacity of the structure against the loads on it.

2. Definition of explosion

An explosion is a sudden, rapid, large-scale release of energy. According to the nature of this type of phenomenon, explosions are classified into three types: physical, nuclear, and chemical. In physical explosions, energy may be released from the

* Corresponding author. Tel.: +989022410579; e-mail: samet.sadeghian@iauc.ac.ir

catastrophic failure of a gas seal or even the fusion of two liquids at different temperatures. In a nuclear explosion, energy is released from the formation of different atomic nuclei by the redistribution of protons and neutrons within the range where the nuclei interact, while the rapid oxidation of fuel elements (carbon and hydrogen atoms) is the main source of energy in chemical explosions.

3. Blast loading

As a result of the explosions, a wave is released from the air, which is known as a shock wave. It is a dense air wave that moves outward from the source of the explosion in a spherical form at a very high speed. In the explosion, there are two important independent parameters, which are the number of explosives that is equivalent to TNT (W) and the distance of the explosives from the structure (R). These two quantities' results are introduced as the Z parameter (scale distance). The use of Z allows us to have a concise and effective expression of the blast wave for a wide range of situations. For example, the Oklahoma bomb in 1995 weighed 1814 kg and R distance of 4.5 meters [3].

$$Z = \frac{R}{W^{1/3}} \quad (1)$$

in which W is the amount of explosives and R is the distance of explosives from the structure.

The observed characteristics of blast waves are influenced by the physical parameters of the blast source. Figure 1 shows the explosion pressure profile. At input time t_A , the pressure position suddenly increases to the overpressure value P_{s0} . Then this pressure decreases to ambient pressure at time t_d , continues to negative pressure (which produces a partial vacuum), and finally returns to ambient pressure at time t_d . The quantity P_{s0} is usually considered the peak pressure.

In the pressure-time diagram, two main stages can be observed: the upper part of the time axis is called the positive stage (up to time t_d), while the part below the time axis is called the negative stage. The negative phase lasts longer and is less intense than the positive phase. When the distance from the explosion source increases, the duration of the positive phase also increases, as a result, the amplitude in this phase decreases. If the amount of explosives is close to the

structure, we will have a larger explosion with more intensity on concentrated parts of the structure, while if the explosives are placed at a distance from the structure, we will have a less intense explosion with a uniform distribution over the entire structure.

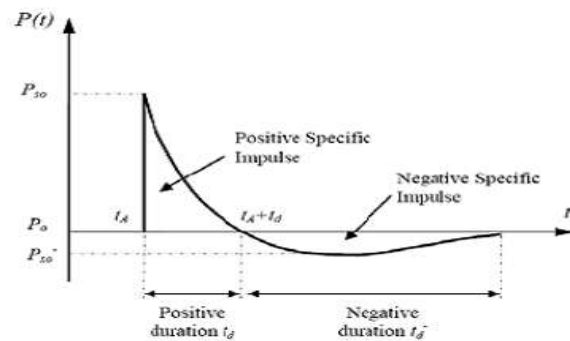


Figure 1 - pressure-time diagram of the blast wave

4. Explosives

The constituent materials of this phenomenon (explosion) can be divided into two primary or secondary types based on their sensitivity to ignition. The primitive type of these materials can be easily detonated by a simple ignition caused by a spark, flame, or impact. Materials such as mercury folinate and lead Azide are examples of this category. When the second type of material bursts (explodes), it produces explosive waves (shocks) that can cause a lot of damage to its surroundings. TNT and ANFO are examples of this type of material [5].

An explosion occurs when a large amount of energy is generally exerted on the explosive. The general characteristics of the explosive substance are determined by using parameters such as the amount of energy, energy density, energy release rate, and the power of the explosive substance. When the explosive material is ideal, regardless of the energy density and power of its source, the explosion can be described using one parameter, the total energy [1].

Before the parameters for an explosion can be derived, the equivalent mass of TNT is required. There are several ways to express the TNT equivalent, but the simplest is the ratio of the mass-specific energy of the actual explosive to the mass-specific energy of TNT. The mass-specific energy of TNT is equal to 6700 kJ/kg. The table below shows the specifications

of some explosives and conversion coefficients to TNT equivalents. According to what was said, in most cases of explosives used for military or industrial purposes, TNT is the reference explosive and the power of the explosive is usually determined by the weight of TNT. In cases where the explosive material is other than TNT, the strength of the explosive material is obtained by using the TNT equivalence factor.

5. Scale rules

The characteristics of the blast wave depend on both the energy released from the explosive and the blast environment. These properties can be measured under controlled conditions in experiments and used as a basis for obtaining information about other explosions using the explosion scaling law. In explosive loading, scaling the characteristics of the blast wave is a common method and several methods have been proposed to estimate the characteristics of the blast wave. By using scaling laws based on laboratory results, it is possible to estimate the characteristics of the explosion wave resulting from the desired value and distance; But assuming full gas and regardless of gravity and viscosity, these laws are not suitable for some strong shock waves or distances close to the explosion source. In the following, two of the most used of these rules are reviewed.

The most common method for scaling the explosion is the Hopkins-Kranz method or the third root, which is shown in Figure 2 [2]. This method was first related by Hopkins in 1915 and later independently by Kranz in 1926 based on the similarity of the wave characteristics of explosions that are at the same scaled distance, when two different explosive charges are made in similar atmospheric conditions.

This law states that two explosive charges of different sizes from the same explosive will produce the same overpressure (P_s) time; which have the same scaled distance (Z) and of course have the same location and atmospheric pressure [5] that is:

$$\frac{R_1}{W_1^{1/3}} = \frac{R_2}{W_2^{1/3}} \quad (2)$$

That is, the explosive charge W_2 in the distance R_2 will create an overpressure equal to the overpressure

of the explosive charge W_1 in the distance R_1 when the above relationship applies.

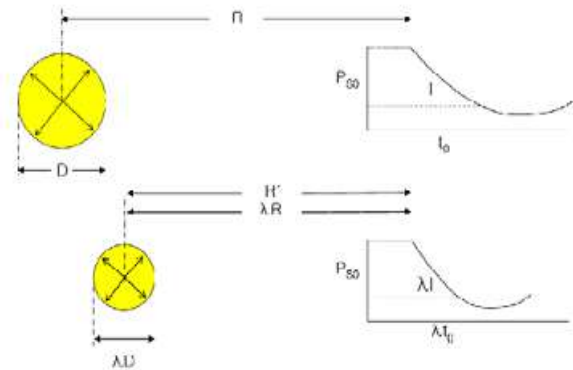


Figure 2- Hopkins-Kranz scale rules

Another one of these laws is the Sachs scaling law. Sachs proposed his relationship in 1944. Based on that, the dimensionless overpressure value according to equation 3 and the dimensionless momentum according to equation 4 can be considered as unique functions of the scaled distance. These equalities are used in equation 5 [2].

$$\bar{P} = \frac{P}{P_0} \quad (3)$$

$$\bar{I} = \frac{ia_0}{E^{1/3}P^{2/3}} \quad (4)$$

$$\bar{R} = \frac{RP_0^{1/3}}{E^{1/3}} \quad (5)$$

In recent relations, a_0 and P_0 are the speed of sound in the atmosphere and the base pressure, respectively.

The studies of Doi and Esparza showed that the Hopkins-Kranz scale is a special case of the Sachs scale [1] In fact, the Sachs scale is the same method as the Hopkins-Kranz scale in the same atmospheric conditions between the laboratory data and the existing conditions.

6. Blast wave reflection

When the blast wave hits a very large rigid surface with a zero-degree impact angle, the direction of airflow in the blast wave is gradually reversed and the static pressure on the surface increases to the reflected pressure, which is called face-on loading. When the reflection process is complete, the reflected wave propagates in the opposite direction from which it

came. The maximum reflected pressure P_r can be obtained using Rankine's relation for an ideal gas [4]:

$$P_r = 2P_s \left[\frac{7P_0 + 4P_s}{7P_0 + P_s} \right] \quad (6)$$

If the C_r coefficient is defined as the ratio of P_r to P_s , we can determine the maximum and minimum values of C_r . When P_s is only slightly greater than atmospheric pressure, the lower limit of C_r will be 2. When P_s is much higher than atmospheric pressure, the upper limit for C_r can reach up to 20.

7. Parameters of the blast wave front

The parameters of the blast wave front are of particular importance. The overpressure profile is usually characterized by parameters such as blast wave arrival time (t_a), explosion base overpressure (P_{s0}) and blast wave transit time (t_0) as shown in Figure 3. These parameters, which are a function of the strength of the explosive material, the distance of the explosion point to the measurement location, and the impact angle, are obtained analytically or experimentally.

The analytical solution of these parameters was first expressed by Hugonit and Rankin to describe shocks in an ideal gas. These equations for the speed of the blast wave front U_s and the maximum dynamic pressure q_s are expressed as follows [4].

$$U_s = \sqrt{\frac{6P_s + 6P_0}{7P_0}} \cdot a_0 \quad (7)$$

$$q_s = \frac{5P_0^2}{2(P_s + 7P_0)} \quad (8)$$

where P_s is atmospheric pressure and a_0 is the speed of sound in air at atmospheric pressure. Broad has provided the following equations to obtain the static overpressure in a spherical explosion [4].

$$P_s = \frac{6.7}{Z^3} + 1 \text{ bar} \quad (P_s > 10 \text{ bar}) \quad (9)$$

$$P_s = \frac{0.975}{Z} + \frac{1.455}{Z^2} + \frac{5.95}{Z^3} - 0.019 \text{ bar} \quad (0.1 < P_s < 10 \text{ bar}) \quad (10)$$

Other parameters of the mass explosion wave are the explosive charge (W) and the actual distance from the center of the explosive to the desired point (R) and the scaled distance (Z), which were explained in the previous sections. Other parameters of the blast wave are: the duration of the positive phase T_s , the positive impact, which is the surface under the pressure-time

diagram from the time t_a to the end of the positive phase:

$$i_s = \int_{t_a}^{t_a + T_s} P_s(t) dt \quad (11)$$

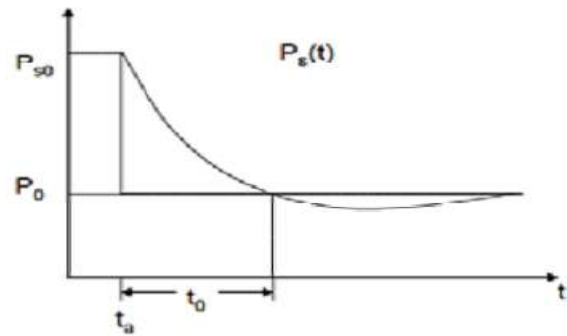


Figure 3- The overall pressure profile due to the wave propagation resulting from the explosion

An example of a pressure-time diagram is shown in Figure 4.

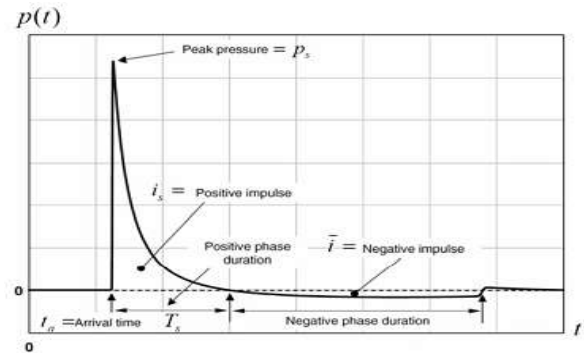


Figure 4 - Pressure history due to a free blast wave in the air

Several methods have been proposed to calculate the explosion parameters. Brad divided the explosion base pressure into two areas Close $P_{s0} > 10 \frac{\text{kgf}}{\text{cm}^2}$ and far $0.1 < P_{s0} < 10 \frac{\text{kgf}}{\text{cm}^2}$. He presented the following relationships to calculate the base pressure of the explosion [4].

$$P_{s0} = \frac{6.7}{Z^3} + 1 \quad (P_{s0} > 10 \text{ kg/cm}^2) \quad (12)$$

$$P_{s0} = \frac{0.975}{Z} + \frac{1.455}{Z^2} + \frac{5.85}{Z^3} - 0.019 \quad (0.1 < P_{s0} < 10 \text{ kg/cm}^2) \quad (13)$$

Brad's relations are in good agreement with the experimental results in the middle and far fields, while

Henry's relations are in good agreement with the experimental results in the near field.

$$P_{s0} = \frac{14.072}{Z} + \frac{5.54}{Z^2} + \frac{0.357}{Z^3} + \frac{0.00625}{Z^4} \quad (0.05 < Z < 0.3) \quad (14)$$

$$P_{s0} = \frac{6.194}{Z} + \frac{0.326}{Z^2} + \frac{2.132}{Z^3} \quad (0.3 < Z < 1.0) \quad (15)$$

$$P_{s0} = \frac{6.662}{Z} + \frac{4.05}{Z^2} + \frac{3.288}{Z^3} \quad (1.0 < Z < 10.0) \quad (16)$$

8. Overpressure profile

When the explosion parameters in the air such as the maximum overpressure P_{s0} , the duration of the positive phase of the explosion t_0 , and the arrival time of the wavefront t_a , as discussed, the profile of the explosion wave can be determined using approximate models such as Flynn's linear model, Etheridge's exponential model and the relation Friedlander calculated [1]. The different states of the blast wave to the surface include three states of surfaces parallel to the movement of the wavefront, surfaces behind the blast wave front, and surfaces opposite to the blast wave front.

9. Simulation and computer programs

In recent years, numerical simulation has become a very important tool in the investigation of an explosion in complex geometries. Many researchers around the world have published results that show the effectiveness of this method. Air3d code has been used to calculate the explosion on urban buildings [6]. Calculation methods in the field of reducing explosion effects are generally divided into two types; Estimation of explosive loads and calculation of structural response to loads.

Computational programs for estimating blast and structural response use both analytical and semi-empirical methods. The programs that use the analytical method are divided into two types coupled analysis and non-coupled analysis. In coupled

analysis, blast simulation is related to structural response. In this type of analysis, Computational Fluid Mechanics (CFD) models are used to estimate blast loads simultaneously with Computational Solid Mechanics (CSM) models for a structural response. Considering the movement of the structure during the calculation of explosive loads, the pressures caused by the movement and damage can be predicted more accurately. Examples of this type of computer code are ABAQUS, LS-DYNA, DYNA3D, and AUTODYN.

The estimation of the load resulting from the explosion in the air can be done through various software. ConWep, AT-Blast, and BlastX can be mentioned in this software. AT-Blast is a tool that can determine the amount of explosive charges in open space. This software allows the user to specify the maximum and minimum range of the explosion, the weight of the explosive material, and the impact angle. This software can calculate the speed, time, pressure, momentum, and duration of the positive phase by getting the information. ConWep software can calculate the effects of conventional weapons of war using the equations and curves in TM5-855-1. This software only can estimate the load resulting from the explosion in the open environment.

10. Summary and conclusion

In this article, the type of explosive loading and parameters related to this type of loading has been investigated. As mentioned, the effects of the explosion in complex environments such as the reflection of multiple blast waves, the negative phase of the wave, etc. can be easily modeled in the codes. CFD modeling. Simplified analytical techniques and semi-empirical methods often ignore these effects. Therefore, the modeling of building groups in dense urban centers can only be done with advanced CFD codes.

11. References

1. Baker, W. E. , *Explosions in air (illustrated ed.)*, University of Texas Press, 1973.

2. Baker, W. E., Cox, P. A., Westine, P. S., Kulesz, J. J., & Strehlow, R. A., *Explosion Hazards and Evaluation*. New York: Elsevier, 1983.
3. Longinow, A., & Mniszewski, K. R. (1996, February). Protecting Buildings against Vehicle Bomb Attacks. *Practice Periodical on Structural Design and Construction*, 1(1).
4. Mays, G. (1995). *Blast Effects on Buildings: Design of Buildings to Optimize Resistance to Blast Loading* (illustrated ed.). (G. Mays, & P. D. Smith, Eds.) London: Thomas Telford.
5. Ngo, T., Mendis, P., Gupta, A., & Ramsay, J. (2007). *Blast Loading and Blast Effects on Structures – An Overview*. *EJSE International Special Issue: Loading on Structures*, 76-91.
6. Rose, T., & Smith, P. (2002, April). Influence of the principal geometrical parameters of straight city streets on positive and negative phase blast wave impulses. *International Journal of Impact Engineering*, 27(4), pp. 359–376.
7. SADEGHIAN, Samet. Retrofit of the Concrete Structures by CFRP Sheets against Explosion. *Journal of Civil Engineering Researchers*, [S.l.], v. 3, n. 1, p. 1-5, nov. 2020. ISSN 2538-516X

Author Guidelines EditEdit Author Guidelines

GENERAL GUIDELINES FOR AUTHORS

Journal of civil engineering researches invites unsolicited contributions of several forms: articles, reviews and discussion articles, translations, and fora. Contributions should fall within the broad scope of the journal, as outlined in the statement of scope and focus. Contributors should present their material in a form that is accessible to a general anthropological readership. We especially invite contributions that engage with debates from previously published articles in the journal.

Submissions are double-blind peer-reviewed in accordance with our policy. Submissions will be immediately acknowledged but due to the review process, acceptance may take up to three months. Submissions should be submitted via our website submission form (see links above for registration and login). Once you login, make sure your user profile has "author" selected, then click "new submission" and follow the instructions carefully to submit your article. If problems arise, first check the FAQ and Troubleshooting guide posted below. If you are still experiencing difficulty, articles can be submitted to the editors as email attachments.

Each article should be accompanied by a title page that includes: all authors' names, institutional affiliations, address, telephone numbers and e-mail address. Papers should be no longer than 10,000 words (inclusive of abstract 100-150 words, footnotes, bibliography and notes on contributors), unless permission for a longer submission has been granted in advance by the Editors. Each article must include a 100 words "note on contributor(s)" together with full institutional address details, including email address. We request that you submit this material (title page and notes on the contributors) as "supplementary files" rather than in the article itself, which will need to be blinded for peer-review.

We are unable to pay for permissions to publish pieces whose copyright is not held by the author. Authors should secure rights before submitting translations, illustrations or long quotes. The views expressed in all articles are those of the authors and not necessarily those of the journal or its editors. After acceptance, authors and Special Issue guest editors whose institutions have an Open Access library fund must commit to apply to assist in article production costs. Proof of application will be requested. Though publication is not usually contingent on the availability of funding, the Journal is generally under no obligation to publish a work if funding which can be destined to support open access is not made available.

Word template and guidelines

Our tailored Word template and guidelines will help you format and structure your article, with useful general advice and Word tips.

(La)TeX template and guidelines

We welcome submissions of (La)TeX files. If you have used any .bib files when creating your article, please include these with your submission so that we can generate the reference list and citations in the journal-specific style

Artwork guidelines

Illustrations, pictures and graphs, should be supplied with the highest quality and in an electronic format that helps us to publish your article in the best way possible. Please follow the guidelines below to enable us to prepare your artwork for the printed issue as well as the online version.

Format: TIFF, JPEG: Common format for pictures (containing no text or graphs).

EPS: Preferred format for graphs and line art (retains quality when enlarging/zooming in).

Placement: Figures/charts and tables created in MS Word should be included in the main text rather than at the end of the document.

Figures and other files created outside Word (i.e. Excel, PowerPoint, JPG, TIFF, EPS, and PDF) should be submitted separately. Please add a placeholder note in the running text (i.e. "[insert Figure 1.]")

Resolution: Rasterized based files (i.e. with .tiff or .jpeg extension) require a resolution of at least 300 dpi (dots per inch). Line art should be supplied with a minimum resolution of 800 dpi.

Colour: Please note that images supplied in colour will be published in colour online and black and white in print (unless otherwise arranged). Therefore, it is important that you supply images that are comprehensible in black and white as well (i.e. by using colour with a distinctive pattern or dotted lines). The captions should reflect this by not using words indicating colour.

Dimension: Check that the artworks supplied match or exceed the dimensions of the journal. Images cannot be scaled up after origination

Fonts: The lettering used in the artwork should not vary too much in size and type (usually sans serif font as a default).

Authors services:

For reformatting your manuscript to fit the requirement of the Journal of Civil Engineering Researchers and/or English language editing please send an email to the following address:

researchers.services@gmail.com

Noted: There is a fixed charge for these mentioned services that is a function of the manuscript length. The amount of this charge will be notified through a reply email.

FAQ AND TROUBLESHOOTING FOR AUTHORS

I cannot log in to the system. How do I acquire a new user name and password?

If you cannot remember your username, please write an email to (journals.researchers@gmail.com), who will locate your username and notify you. If you know your username, but cannot remember your password, please click the "Login" link on the left-hand menu at homepage. Below the fields for entering your username and password, you will notice a link that asks "Forgot your password?"; click that link and then enter your email address to reset your password. You will be sent an automated message with a temporary password and instructions for how to create a new password. TIP: If you do not receive the automated email in your inbox, please check your SPAM or Junk Mail folder. For any other issues, please contact our Managing Editor, Kamyar Bagherinejad (admin@journals-researchers.com).

How do I locate the online submission form and fill it out?

First you need to register or login (see above). Once you are logged in, make sure the "roles" section of your profile has "Author" selected. Once you assign yourself the role of "Author," save your profile and then click the "New Submission" link on your user home page.

Once you arrive at the submission form page, please read the instructions carefully filling out all necessary information. Unless specified otherwise by the editors, the journal section to be selected for your submission should be "Articles." Proceed to the remaining sections, checking all boxes of the submission preparation checklist, and checking the box in the copyright notice section (thus agreeing to journals-researchers's copyright terms). Once the first page is completed, click "Save and Continue." The next page allows you to upload your submission. Use the form to choose your file from your computer. Make sure you click "Upload." The page will refresh and you may then click "Save and Continue." You will then proceed to a page for entering the metadata for your article. Please fill out all required fields and any further information you can provide. Click "Save and Continue." The next page allows you to upload supplementary files (images, audiovisual materials, etc.). These are not required, but if you wish to provide supplementary materials, please upload them here (do not forget to click "Upload." Then click "Save and Continue." This brings you to the final page of the submission form. Please click "Finish Submission" in order to close the

submission process. You will then be notified by email that your article has been successfully submitted. TIP: If you do not receive the automated email in your inbox, please check your SPAM or Junk Mail folder. For any other issues, please contact our Managing Editor, Kamyar Bagherinejad (admin@journals-researchers.com).

Why am I not receiving any email notifications from HAU?

Unfortunately, some automated messages from Open Journal Systems arrive in users' Spam (or Junk Mail) folders. First, check those folders to see if the message was filtered into there. You may also change the settings of your email by editing your preferences to accept all mail from [jcer] and related journals-researchers.com email accounts.

I am trying to upload a revised article following an initial round of peer-review, but I cannot locate where to upload the article. Where do I submit a revised article?

Follow the login process outlined above and when you successfully login you will see on your user home page a link next to "Author" for "active" articles in our system (usually it is only one article, but if you have multiple submissions currently in our system, the number could be higher. Click the "Active" link and you will be led to a page that lists your authored articles currently in our system. Click the link under the column labeled "Status" and this will take you to a page showing the current review status of your article. At the very bottom of the screen, you will see an upload form under the heading "Editor decision." Here you may upload your revised article. An automated email will be sent to the editors and you may also notify them directly via email. You may then logout.

I successfully submitted an article; how long will it take for the editors to respond to me with a decision.

For all articles that are recommended for peer-review, the editors of JCER strive to notify authors of a decision within 4-6 weeks. You may contact JCER's Managing Editor, Kamyar Bagherinejad (admin@journals-researchers.com). if you have any questions relating to the review process and its duration.

For all other inquiries, please contact: Kamyar Bagherinejad (Managing Editor)

Privacy Statement

The names and email addresses entered in this journal site will be used exclusively for the stated purposes of this journal and will not be made available for any other purpose or to any other party.

Articles

Section default policy

Make a new submission to the Articles section.

Copyright Notice EditEdit Copyright Notice

Journal of Civil Engineering Researchers follows the regulations of the International Committee on Publication Ethics (COPE) and the ethical principles of publishing articles in this journal are set based on the rules of this committee, and in case of problems, it will be treated according to these rules.

This work is licensed under a Creative Commons Attribution 4.0 International License (CC BY 4.0).

In short, copyright for articles published in this journal is retained by the authors, with first publication rights granted to the journal. By virtue of their appearance in this open access journal, articles are free to use, with proper attribution and link to the licensing, in educational, commercial, and non-commercial settings

Privacy Statement EditEdit Privacy Statement

The names and email addresses entered in this journal site will be used exclusively for the stated purposes of this journal and will not be made available for any other purpose or to any other party.

Scholars Pavilion



Scholars Pavilion or **Scholars Chartagi** is a monument donated by the Islamic Republic of Iran to the United Nations Office at Vienna. The monument architecture is claimed by the Islamic Republic News Agency of Iran to be a combination of Islamic and Achaemenid architecture, although the latter clearly predominates in the decorative features, with Persian columns and other features from Persepolis and other remains from the Achaemenid dynasty. The Chahartaq pavilion form runs through the architecture of Persia from pre-Islamic times to the present.

Statues of four famous Persian medieval scholars, Omar Khayyam, Al-Biruni, Muhammad ibn Zakariya al-Razi and Ibn-Sina are inside the pavilion. This monument donated in June 2009 in occasion of Iran's peaceful developments in science.

